Solar Array Synthesis Computer Program

by
T.J. Faith
RCA, Astro-Electronics Division
Princeton, New Jersey

Prepared for
National Aeronautics and Space Administration
Goddard Space Flight Center
Greenbelt, Maryland 20771

NAS5-21642

APR 1973

RCA

RCA | Government and Commercial Systems
Astro Electronics Division | Princeton, New Jersey

Solar Array Synthesis Computer Program

by
T.J. Faith
RCA, Astro-Electronics Division
Princeton, New Jersey

Prepared for
National Aeronautics and Space Administration
Goddard Space Flight Center
Greenbelt, Maryland 20771

NAS5-21642

RCA | Government and Commercial Systems
Astro Electronics Division | Princeton, New Jersey

ABSTRACT

Empirical equations have been derived from measurements of solar cell photovoltaic characteristics relating open circuit voltage, V_O, light generated current, I_L, cell series resistance, R_S, and current-voltage characteristic to cell temperature, T, intensity of illumination, W, and 1 MeV electron fluence, ϕ. The experimental results covered the ranges; $123°K \leq T \leq 473°K$, $5\ mW/cm^2 \leq W \leq 1830\ mW/cm^2$ and $1 \times 10^{13}\ e/cm^2 \leq \phi \leq 1 \times 10^{16}\ e/cm^2$. Both 10 Ω-cm and 1 Ω-cm n/p cells degrade in V_O at a rate proportional to $\phi^{0.25}$. At 273°K, I_L degrades at a rate proportional to $\phi^{0.153}$. The normalized temperature coefficient of I_L varies as $\phi^{0.18}$ for temperatures above approximately 273°K and is independent of fluence at lower temperatures. For $T \geq 223°K$ the temperature coefficient of V_O in 10 Ω-cm cells is, to a good approximation, constant at 0.0023 V/°K independent of T, W, and ϕ; the same value applies to 1 Ω-cm cells except for $\phi \leq 1 \times 10^{14}\ e/cm^2$ where the value is 0.0022/°K. The illumination dependence of I_L is approximately linear. However, the values of I_L at 560 mW/cm^2 illumination are approximately 3.7 times those at 140 mW/cm^2 approximately 10 percent below the expected factor of 4. This could be due to an uncertainty in neutral-density filter transmission. Open-circuit voltage increases logarithmically with illumination intensity; for 1Ω-cm cells V_O increases approximately 0.032V per decade increase in W, the corresponding value for 10Ω-cm cells in 0.025V. An equation for the I-V curve, valid for $223°K \leq T \leq 373°K$ and $35\ mW/cm^2 \leq W \leq 560\ mW/cm^2$, was generated for 10 Ω-cm cells by adding a series resistance term to the illumination-dependent equation for V_O. The series resistance increased logarithmically with fluence, linearly with $V_O - V$, and also displayed temperature and illumination dependencies.

TABLE OF CONTENTS

Section			Page
I	INTRODUCTION		1
II	EXPERIMENTAL DETAILS		3
	A.	Solar Cells and Text Matrix	3
	B.	Cell Test Apparatus	5
	C.	Calibration of Illumination Intensity	5
	D.	Cell Irradiation	7
	E.	Measurement Problems and Solutions	8
		1. High Temperature, High Illumination	8
		2. Low Temperature	8
		3. Test Sequence	9
III	RESULTS AND ANALYSIS		11
	A.	Approach	11
	B.	Light-Generated Current	11
		1. Measurement Uncertainties	11
		2. Data and Empirical Equations	15
	C.	Open Circuit Voltage	30
		1. Measurement Uncertainties	30
		2. Data and Empirical Equations	31
		3. Voltage Anomaly at Low Temperature	40
	D.	Curve Shape	41
		1. Range of Analysis	41
		2. Equation Format	42
		3. Series Resistance	43
		4. Curve-Shape Temperature Dependance	49
IV	CONCLUSIONS		53
V	ACKNOWLEDGEMENTS		55
VI	REFERENCES		57
VII	APPENDIX		59

LIST OF ILLUSTRATIONS

Figure		Page
1	Temperature-Illumination Combinations at which Cells were Measured	3
2	Photovoltaic Characteristic at High Cell Temperature and High Illumination Intensity	9
3	Light Generated Current Before and After 473° K Anneal	13
4	Distribution of Pre-Irradiation Values of Light Generated Current	14
5	Fluence Dependence of the Parameter δ_I	16
6	Light Generated Current vs. Fluence at 273° K and 140 mW/cm² Illumination, 10 Ω-cm Cells	18
7	Light Generated Current vs. Fluence at 273° K and 140 mW/cm² Illumination, 1 Ω-cm Cells	18
8	Normalized Temperature Coefficient of Light Generated Current Versus Fluence	19
9	Light Generated Current at W = 140 mW/cm² Versus Cell Temperature and Fluence, 10 Ω-cm Cells	21
10	Light Generated Current at W = 140 mW/cm² Versus Cell Temperature and Fluence, 10 Ω-cm Cells	21
11	Light Generated Current at W = 140 mW/cm² Versus Cell Temperature and Fluence, 1 Ω-cm Cells	21
12	Light Generated Current at W = 140 mW/cm² Versus Cell Temperature and Fluence, 1 Ω-cm Cells	21
13	Light Generated Current at W = 35 mW/cm² Versus Cell Temperature and Fluence, 10 Ω-cm Cells	23
14	Light Generated Current at W = 35 mW/cm² Versus Cell Temperature and Fluence, 1 Ω-cm Cells	23
15	Light Generated Current at W = 5 mW/ cm² Versus Cell Temperature and Fluence, 10 Ω-cm Cells	24
16	Light Generated Current at W = 560 mW/cm² Versus Cell Temperature and Fluence, 10 Ω-cm Cells	26
17	Light Generated Current at W = 560 mW/cm² Versus Cell Temperature and Fluence, 1 Ω-cm Cells	26

LIST OF ILLUSTRATIONS (Continued)

Figure		Page
18	Light Generated Current at W = 1830 mW/cm² Versus Cell Temperature and Fluence, 10 Ω-cm and 1 Ω-cm Cells	27
19	Divergence of I_L Values of Empirical Equations from Experimental I_L Values, 10 Ω-cm Cells	29
20	Divergence of I_L Values of Empirical Equations from Experimental I_L Values, 1 Ω-cm Cells	30
21	Distribution of Pre-Irradiation Values of Open Circuit Voltage	31
22	Fluence Dependence of the Parameter δ_V	32
23	Open Circuit Voltage Versus Cell Temperature and Illumination at $\phi = 1\times10^{13}$ e/cm², 10 Ω-cm Cells	34
24	Open Circuit Voltage Versus Cell Temperature and Illumination at $\phi = 3\times10^{14}$ e/cm², 10 Ω-cm Cells	34
25	Open Circuit Voltage Versus Cell Temperature and Illumination at $\phi = 3\times10^{15}$ e/cm², 10 Ω-cm Cells	35
26	Open Circuit Voltage Versus Cell Temperature and Illumination at $\phi = 1\times10^{16}$ e/cm², 10 Ω-cm Cells	35
27	Open Circuit Voltage Versus Cell Temperature and Illumination at $\phi = 1\times10^{13}$ e/cm², 1 Ω-cm Cells	36
28	Open Circuit Voltage Versus Cell Temperature and Illumination at $\phi = 3\times10^{14}$ e/cm², 1 Ω-cm Cells	36
29	Open Circuit Voltage Versus Cell Temperature and Illumination at $\phi = 3\times10^{15}$ e/cm², 1 Ω-cm Cells	37
30	Open Circuit Voltage Versus Cell Temperature and Illumination at $\phi = 1\times10^{16}$ e/cm², 1 Ω-cm Cells	37
31	Divergence of V_O Values of Empirical Equations from Experimental V_O Values, 10 Ω-cm Cells	39
32	Divergence of V_O Values of Empirical Equations from Experimental V_O Values, 1 Ω-cm Cells	40
33	Photovoltaic Curves Showing the Effect of a Schottky Barrier at Low Cell Temperature	41
34	Open Circuit Voltage Versus Light Generated Current at Several Fluences and Cell Temperatures, 10 Ω-cm Cells	43

LIST OF ILLUSTRATIONS (Continued)

Figure		Page
35	Illustration of Method for Calculating R_s	44
36	R_s at 560 mW/cm² Versus Position on the Solar Cell Photovoltaic Characteristic, T=273° K	45
37	R_s at 560 mW/cm² Versus Position on the Solar-Cell Photovoltaic Characteristic, T=373° K	45
38	R_s Versus Fluence and Cell Temperature, W=560 mW/cm²	46
39	R_s Versus Fluence and Cell Temperature, W=140 mW/cm²	46
40	R_s Versus Fluence and Cell Temperature, W=35 mW/cm²	47
41	Illustration of Fit Between Empirical and Experimental I-V Curves	48
42	Photovoltaic Characteristics at W=35 mW/cm², $\phi = 3\times 10^{14}$ e/cm²	49
43	Photovoltaic Characteristics at W=140 mW/cm², $\phi = 3\times 10^{14}$ e/cm²	50
44	Photovoltaic Characteristics at W=140 mW/cm², $\phi = 1\times 10^{16}$ e/cm²	50
45	Constructed Photovoltaic Characteristics (using A=1.36)	51

LIST OF TABLES

Table		Page
1	Solar Cell Post-Irradiation Measurement Sequence	10
A-1	Index Numbers and Corresponding Values for the Parameters, T, W, and ϕ	60

I. INTRODUCTION

This is the final report on Contract NAS5-21642, the purpose of which is to update and expand the range of applicability of the Solar Array Synthesis Computer Program developed by RCA under contract to NASA-GSFC and described in GSFC Technical Report No. X-716-69-390 and RCA Final Report, Contract NAS5-11669, issued 1 February 1970. The temperature (T) and illumination-intensity (W) ranges of this program, which predict solar array degradation in the space environment, have been extended to $123^{\circ}K \leq T \leq 473^{\circ}K$ and $5\ mW/cm^2 \leq W \leq 1830\ mW/cm^2$ by measurements of solar cell current-voltage characteristics for 24 temperature-illumination combinations spanning these ranges. The measurements were made on both 10 Ω-cm and 1 Ω-cm n/p silicon solar cells irradiated by 1 MeV electrons to fluences from $1 \times 10^{13}\ e/cm^2$ to $1 \times 10^{16}\ e/cm^2$ and on unirradiated cells. The experimental data has been analyzed and empirical equations have been derived to describe light generated current, open circuit voltage, cell series resistance, and current-voltage curve as functions of cell temperature, illumination, and 1 MeV electron fluence.

II. EXPERIMENTAL DETAILS

A. SOLAR CELLS AND TEST MATRIX

The solar cells used in these experiments were 1cm × 2cm commercial grade n/p silicon cells with Ti-Ag solderless contacts. The manufacturer was Centralab. Two resistivities, 1 Ω-cm* and 10 Ω-cm, were tested. The experimental test matrix encompassed three variables; cell temperature, T, illumination intensity, W, and 1 MeV electron fluence, ϕ. Photovoltaic (I-V) characteristics were taken on all cells for the temperature-illumination matrix shown in Figure 1 after irradiation to the following fluences: 0, 1×10^{13}, 3×10^{13}, 1×10^{14}, 3×10^{14}, 1×10^{15}, 3×10^{15}, and 1×10^{16} e/cm^2. As is seen from Figure 1 the cells were measured at 50°K intervals from 123°K to 473°K (-150°C to +200°C) at three of the following intensities: 5, 35, 140, 560 and 1830mW/cm^2. In addition the cells were measured prior to irradiation using an attenuated T, W matrix covering the ranges: 173°K ≤ T ≤ 373°K; 5mW/cm^2 ≤ W ≤ 140mW/cm^2.

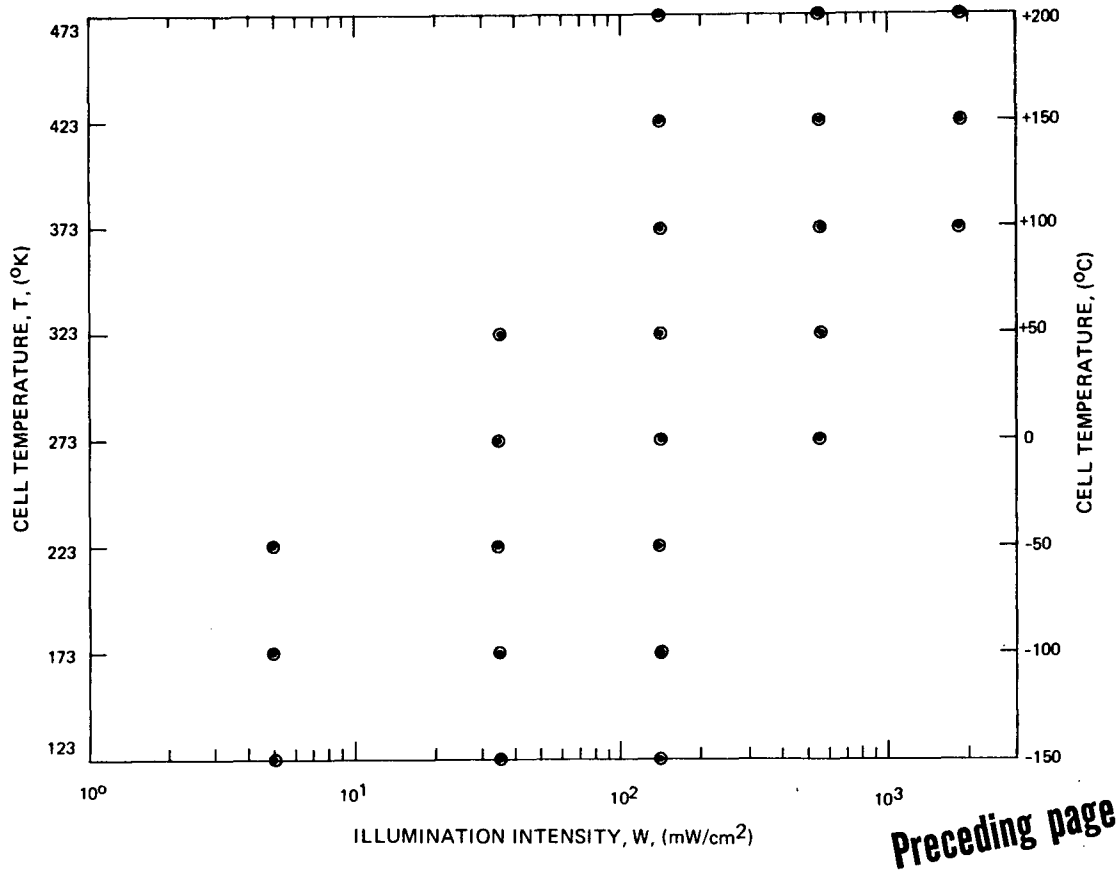

Figure 1. Temperature-Illumination Combinations at which Cells were Measured

*It is noted that capacitance measurements on the nominal 1Ω-cm cells indicated a base doping level closer to 2 Ω-cm.

Five cells of each resistivity were tested at each fluence, giving a total of 80 test cells (40 each of 1 Ω-cm and 10 Ω-cm cells). Each set of 5 cells was tested over the entire temperature range. This approach, which was chosen over the alternative approach of using different cell sets at low and high temperature, had the advantage of economy and consistency but gave rise to problems of cell compatibility and survival over the temperature extremes encountered (as discussed below).

Prior to testing, the cells were mounted on 2" × 3" × 1/16" kovar cell blocks plated with approximately 0.0002" of copper for good electrical conductivity and solderability. The cells were soldered to the blocks using a minimum amount of soft (Pb-Sn) solder with 2 percent silver additive (to bring the solder melting temperature up to 480°K). Each block carried six cells (3 rows of 2 cells), five of which were test cells, the sixth being a dummy cell to whose top contact was soldered a copper-constantan thermocouple. Electrical connections to the top contacts of the test cells were made using flexible silver mesh. All test cells had 4-probe contacts to avoid a voltage drop across the series resistance in the voltage leads. The first set of pre-irradiation measurements found the majority of cells cracking under thermal strain at the lowest cell measurement temperature, 123°K. This dictated that the pre-irradiation measurements not extend below 173°K and that post-irradiation measurements at 123°K be made only after the completion of measurements at all other temperatures. (The test sequence adopted, the consequent problems, and their solutions are discussed in part E of this section.)

For photovoltaic measurements the solar-cell blocks were mounted on a copper finger which was attached to a liquid nitrogen dewar. An electrical heater mounted on the back surface of the finger provided active temperature control over the entire range of the measurements. The cold finger dewar assembly was positioned in an air tight vessel which was evacuated during low temperature tests to avoid condensation and icing, and filled with dry nitrogen during high temperature tests to inhibit outgassing of the vacuum and thermal-contact greases present inside the vessel. A 3" diameter, 1/4" thick Corning 7940 fused silica disc with flat optical transmission from 0.4 μm to 1.2 μm provided a sight glass for cell illumination inside the air tight vessel. The electrical leads from the test cells and heater, and the thermocouple leads from the dummy cells were brought out from the cold finger dewar assembly through electrical feedthrus in the top of the assembly. The entire assembly, including vacuum pump and standard cell (described in part C, this section), was positioned on a table fitted with wheels to enable transverse and axial movement with respect to the illuminator.

B. CELL TEST APPARATUS

The source of illumination used in the experiments was an Aerospace Controls Corporation model 302 xenon arc solar simulator with a spectral intensity match to AMO intensity Johnson spectrum[1] given by the following deviations for the corresponding spectral bands: -15.3% for the band extending from 0.40 to 0.45 μm; -2.5% for 0.45 to 0.50 μm; -5.9% for 0.50 to 0.60 μm; +5.6% from 0.60 to 0.70 μm; +5.3% from 0.70 to 0.80 μm; +6.5% from 0.80 to 0.90 μm; +14.4% from 0.90 to 1.00 μm; and -4.5% from 1.0 to 1.2 μm. The intensity of illumination at the test plane could be varied continuously by adjusting either the xenon arc current or the distance between the arc and the test plane. Low intensity illumination (5 and 35mW/cm^2) was accomplished using a set of neutral density filters purchased from Aerospace Controls Corporation. Low frequency plasma oscillations in the xenon arc of the simulator caused considerable difficulty. These oscillations, at approximately 2Hz and 40Hz caused up to 3 percent ripple in beam intensity. By judicious choice of arc current and forced air cooling rates for the xenon bulb this ripple was reduced to approximately 1.5 percent. However, the presence of the oscillation, and occasional increases in its amplitude necessitated continuous monitoring and adjustment of the intensity on a standard cell during the measurements.

Photovoltaic current-voltage characteristics were generated automatically by a Spectrolab model D550 electronic load and displayed on a Moseley model 7030A X-Y recorder. Open-circuit voltage and short-circuit current were displayed on a NLS model 3020 digital voltmeter, the voltmeter being shunted by an SRI precision 1 ohm resistor for the current display. Cell temperature was measured using a Rubicon model 2745 potentiometer in conjunction with the aforementioned copper-constantan thermocouple soldered to the dummy cell.

C. CALIBRATION OF ILLUMINATION INTENSITY

Intensity of illumination was calibrated using an AIEE-mounted Heliotek standard cell whose current output was measured at Table Mountain, Ca. and extrapolated to 63.1mA at Air Mass Zero illumination (140mW/cm^2) using results of balloon standard cell measurements[2]. The standard cell was mounted beside the cell block location, 3 inches from the center of the block, and in the same test plane. Since the test cells view the illuminator through a sight glass a companion sight glass was placed in front of the standard to equalize the transmission to the standard and the test cells. The standard cell temperature was maintained at 30°C using a circulating brine system.

Short-circuit current of the standard cell was measured with a model 825A Flukemeter shunted by an SRI 1 ohm precision resistor. After a scan was performed to determine beam uniformity* the illuminator axis was positioned to provide equal intensity at test cell and standard cell position.

To establish a beam intensity of 140mW/cm^2 at the test cell location the xenon arc current and illuminator-to-cell distance were adjusted to yield a standard cell current of 63.1mA. For lower illumination intensities neutral density filters were inserted in the simulator beam. To obtain intensity W, a filter combination which gave a standard-cell current of 63.1 W/140 was chosen.

To achieve high intensities (initially established at nominal values of 650mW/cm^2 and 2100mW/cm^2) it was necessary to move the test plane closer to the illuminator, consequently decreasing the beam size. The beam no longer spanned the 3 inches between the test cells and standard cell, prohibiting simultaneous test-cell and standard-cell measurement. However a double mirror system enabled fast diversion of the beam from test cells to the standard cell and standard measurements were made within approximately 10 seconds, both before and after each test-cell current measurement.

To establish high intensity, W, the standard cell was centered on the beam axis and a filter combination with transmission equal to 140/W was placed in the beam. Xenon arc current and distance were adjusted to yield a standard current of 63.1mA. Removal of the filters then established the illumination intensity at W. (An additional set of measurements provided the proper adjustment required to relate the standard current on-axis to that obtained through beam diversion with the test cells on axis.) The above calibration procedure in principle avoids the necessity of assuming a linear current-intensity relationship in this high intensity region. What was required was an accurate knowledge of the transmission of the filters.

Two sets of filters were used, one set having manufacturer-specified transmission of 0.217; the other, 0.067, resulting in apparent intensities of 645 and 2090 mW/cm^2, respectively. However, it was observed during the calibration measurements that, starting with (unfiltered) intensity of 140 mW/cm^2, inserting a filter with manufacturer-specified transmission, t, did not result in a standard-cell current of 63.1t. Rather, the current was consistently above 63.1t indicating higher transmission coefficients than the specified values. To check this observation, two tests were performed, 1) spectral transmission of the filters was measured on a Perkin Elmer model 350 spectrophotometer and 2) transmission measurements from short-circuit current ratio were made using six different solar cells. The spectrophotometer measurements showed

*Beam uniformity - center to edge - was found to be within the 5 percent claimed by the simulator manufacturer. The beam is a square approximately 8 inches on a side at 140 mW/cm^2.

the spectral transmission of the filters to be reasonably flat and equal to the specified values within a few percent. However the current ratios obtained on the six cells were in good agreement with each other, yielding higher transmission coefficients than the spectrophotometer. A possible explanation for this is that the filter transmission is dependent on the incident light intensity, the intensity of the spectrophotometer illumination being several orders of magnitude below that from the cell illuminator. Since the filters were used at illuminator (high) intensities, the current ratio values were used for the transmission coefficient. The resulting intensities are 560 mW/cm^2 and 1830 mW/cm^2.

Another question regarding the filters concerns a possible wavelength dependence of transmission coefficient with high incident light intensity. Such a dependence would be important mainly at 5 and $35 mW/cm^2$ since at these intensities filters are in the light beam during test-cell measurement. A gross indication concerning its presence or absence can be obtained by comparing the illumination-dependent current ratio at different fluences. If the filter transmission is wavelength dependent the current ratio will change with fluence since the shape of spectral response curve of the cell is fluence dependent. For both illuminations the current ratio was reasonably constant indicating that the filters used at these intensities had reasonably flat spectral transmissions.

D. CELL IRRADIATION

One test-cell block of each resistivity (1 and 10 Ω-cm) was irradiated to each of the following fluences of 1 MeV electrons: 1×10^{13}, 3×10^{13}, 1×10^{14}, 3×10^{14}, 1×10^{15}, 3×10^{15} and $1 \times 10^{16} e/cm^2$. The irradiations were performed at the RCA Laboratories 1 MeV Van de Graaff generator in Princeton, N.J. Fluence measurements were made using a Faraday-cup detector connected to a current integrator. The cell blocks were mounted during irradiation on a rotating wheel with three holes around its circumference to enable passage of the beam to the Faraday cup. The wheel rotation rate being approximately 3 r/min, the beam was sampled approximately every 7 seconds. Using this technique the error introduced by beam non-uniformities and temporal variations was minimized. The resulting fluence measurements are estimated to be accurate to within 5 percent. The cell temperature was approximately 300°K during irradiation, illumination was provided by a 500W tungsten lamp (estimated intensity at cell surface: $30 mW/cm^2$), and the cell terminals were unconnected. The average irradiation rates were $4 \times 10^{13} e/cm^2$-min for the heavier irradiations ($\phi \geq 10^{14} e/cm^2$) and $4 \times 10^{12} e/cm^2$-min for the two lowest fluences (1×10^{13} and $3 \times 10^{13} e/cm^2$).

E. MEASUREMENT PROBLEMS AND SOLUTIONS

1. High Temperature, High Illumination

Several problems are inherent to the wide range of temperatures and intensities covered in this experiment. No single cell design is compatible with such a range, and the present cells, being utilized mainly for earth-orbiting missions are designed for operation at 140mW/cm^2 at temperatures between approximately 220°K to 350°K. Cells designed specifically for high temperature, high-illumination applications [3,4] have low base resistivity ($\lesssim$ 1 Ω-cm), deep-diffused junctions, and many contact fingers to maximize open-circuit voltage and minimize series resistance. The series resistance problem is particularly severe at high temperature and the effect of high illumination can be illustrated by considering the voltage drop across a 1 Ω series resistance in a cell illuminated by 2000mW/cm^2 and consequently having a light-generated current of approximately 1A. Because of the IR drop, the terminals of such a cell must be driven 1V negative to establish zero bias across the n/p junction. At zero terminal voltage, the junction is positively biased, resulting in a short-circuit current significantly below the light-generated current. The light-generated current is the more basic parameter, and the value of the short-circuit current will approach the light-generated current in a cell designed for high temperature operation. Therefore the currents reported herein will be the light-generated current whenever the two currents are unequal. Figure 2, which gives two identical photovoltaic I-V plots with different voltage sensitivities, illustrates the method of obtaining the light-generated current. Curve (a) is the standard photovoltaic curve, generated for positive cell bias only, curve (b) is extended to negative bias. The curves give short-circuit current values of 250mA, but curve (b) shows the current leveling off at 910mA, which is the light-generated current, I_L. The I_L value is thus approached in this (typical) case only by driving the cell terminal voltage 1.5V negative. The short-circuit current, I_{sc}, is less than one third of I_L. The large number of measurements taken in these experiments show little coherence in the I_{sc} values (due to strong dependence on series resistance, which varies from cell to cell) but a good deal of coherence in the I_L data as will be seen in section III, below. The temperature/illumination combinations for which I_{sc} does not equal I_L are, 473°K/140, 560 and 1830mW/cm^2, 423°K/560 and 1830mW/cm^2, and 373°K/1830mW/cm^2. For all other T, W combinations measured, $I_{sc}=I_L$.

2. Low Temperature

The diode characteristic in solar cells diverges from the ideal diode behavior, the effect being especially important at low temperature and low illumination intensities. Large degradations in cell output have been ascribed to surface leakage currents across the junction[5] which results in poor curve shapes and in open-circuit voltage loss[6-9]. This being a property of the individual cells there is no way to avoid this problem short of pre-selecting the cells after preliminary low temperature measurements.

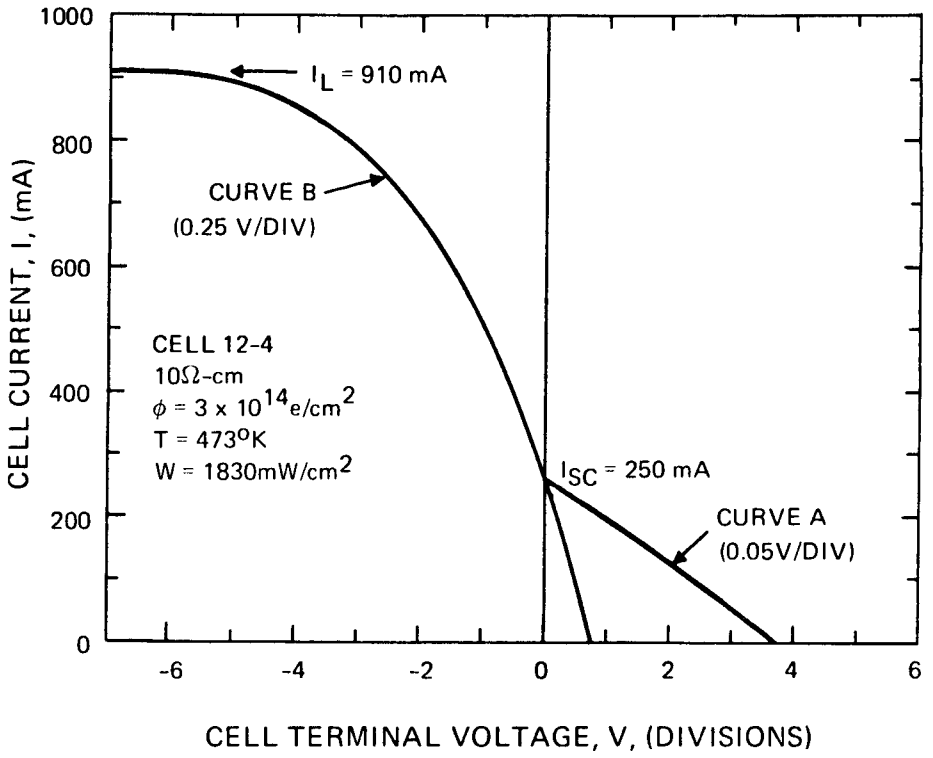

Figure 2. Photovoltaic Characteristic at High Cell Temperature and High Illumination Intensity

At low temperature a rectifying Schottky barrier often forms at the cell back contact causing a loss in open-circuit voltage and degrading the I-V curve shape. This can be eliminated[9] by using cells with a heavily doped p^+ region adjacent to the back contact. Unfortunately, the cells used in these experiments had no such region and Schottky barriers were encountered in most cells at the two lowest measurement temperatures, 123°K and 173°K, invalidating the voltage readings at these temperatures.

3. Test Sequence

As mentioned previously, extensive cell breakage occurred during preliminary measurements at 123°K. Consequently it was decided that the post-irradiation measurements would proceed in temperature upward from 273°K, low temperature measurements being made only after the measurements at 473°K. This was in contrast to the originally-planned sequence which would have started at 123°K and proceeded upward in temperature, the 473°K measurements being performed last.

The original sequence would have avoided the effects of any high temperature annealing. The revised sequence, in contrast, had the disadvantage that the low temperature (223°K, 173°K, and 123°K) measurements were taken only after the cell had been at elevated temperatures where significant annealing of radiation damage could occur. An attempt to account for this was made in choosing the post-irradiation measurement schedule outlined in Table I. Measurements 1 to 5 and 10 to 12 covered the T, W matrix as outlined in Figure 1. Measurements 6 to 9, taken for W=140mW/cm^2 and moving downward in temperature provided a quantitative measure of the degree of annealing which occurred while the cell was at elevated temperature. This provided a basis for adjustment of the currents measured at low temperature to compensate for the annealing. This will be described in detail in section III.

TABLE I. SOLAR CELL POST-IRRADIATION MEASUREMENT SEQUENCE

Measurement No.	Cell Temperature (°K)	Illumination Intensities $\left(\frac{mW}{cm^2}\right)$
1	273	35, 140, 560
2	323	35, 140, 560
3	373	140, 560, 1830
4	423	140, 560, 1830
5	473	140, 560, 1830
6	423	140
7	373	140
8	323	140
9	273	140
10	223	5, 35, 140
11	173	5, 35, 140
12	123	5, 35, 140
13	273	140

III. RESULTS AND ANALYSIS

A. APPROACH

Analysis of the experimental data was initiated at the endpoints of the I-V curve, i.e., at open-circuit voltage, V_O, and light-generated current, I_L. Empirical relationships were obtained for these two parameters as functions of cell temperature, illumination and fluence. Since five cells were measured for each experimental condition the raw data for the analysis were the values averaged over the five cells, unless otherwise specified. In deriving analytical equations to fit the data two principle guidelines were followed: 1) generate the minimum number of equations compatible with an acceptably good fit (as dictated by uncertainties and scatter in the raw data), and 2) seek a similar format for relationships for 1 Ω-cm and 10 Ω-cm cells to facilitate system comparisons between the two resistivities.

Having obtained relationships for V_O and I_L, the I-V curves were analyzed in detail (for 10 Ω-cm cells) by proceeding downward along the curve from the V_O endpoint. This method had the advantage of starting at the point on the curve where the voltage drop due to cell series resistance vanished. Since V_O was measured at three different illuminations for each fluence and cell temperature, it was possible to construct an I-V characteristic by adding a series resistance term to an empirical equation relating V_O to I_L. The method and results are described in part D of this section, following the results of the light-generated current and open-circuit voltage analyses, which are presented in parts B and C, respectively.

B. LIGHT-GENERATED CURRENT

1. Measurement Uncertainties

To establish criteria concerning what constitutes a satisfactory fit to the data, the sources of uncertainty in the measurements and cell-to-cell variations were considered. A fluctuation in the light source used to illuminate the cells represented a source of experimental error. The xenon arc, as noted in section II, had oscillations at approximately 2 Hz and 40 Hz which caused peak-to-peak fluctuations in illumination of approximately 1.5 percent. For measurements at 5, 35, and 140 mW/cm^2 illumination, this source of error was eliminated by simultaneous readings on the standard cell and test cell. Simultaneous readings were not possible at intensities of 560 and 1830 mW/cm^2 because of the reduced beam size. Estimates based on repeated measurements between the standard and test cells and on the amplitude of oscillation, indicated an error at these two intensities of approximately ±0.5 percent due to this fluctuation.

Another possible source of error is long-term drift in the output of the illuminator. It is believed that this was largely eliminated by frequent monitoring of the standard cell. Periodic measurements over several days (approximate duration of the entire measurement sequence on a given cell block) indicated reproducibility within ± 1 percent.

The deviation of the spectral intensity of the illuminator from the AMO spectrum represents another source of error. The evaluation of its effect, however, is a complex undertaking beyond the scope of the present work. The percents deviation from Johnson spectrum[1] bands covering the 0.4 to 1.2 μm wavelength region are listed in section II of this report. An additional source of error in the illuminator system is due to the neutral density filters which introduce an uncertainty in the effective intensity of illumination at intensities other than 140mW/cm^2. This factor was discussed in section IID.

Cell current being temperature dependent, an uncertainty in cell temperature represents a source of error. As will be seen below (in Figure 8) the fractional change in cell current varies from approximately 0.07%/°K in unirradiated cells to 0.25%/°K in heavily irradiated cells. During cell measurements the temperature, as measured at the dummy cell, was maintained within ± 2°K of the nominal value. Since the effective thermal conductivity of the cell mounting system was high (see section II) it is estimated that the dummy-cell temperature is the same as that of the test cells within ± 1°K. Consequently, the cell-temperature uncertainty is ± 3°K resulting in current uncertainties ranging from approximately ± 0.2 percent in lightly irradiated cells to ± 0.8 percent in heavily irradiated cells.

Cell annealing, which can occur at the high-temperature end of the measurement sequence, changes the physical properties of the cells thereby introducing an error in subsequent measurements. Electron irradiated cells of the type used in these experiments experience little annealing below about 423°K, however, a reverse annealing stage has been observed [10] between 423°K and 473°K. During this stage the current of the cell is generally reduced from the post-irradiation value. Since the post-irradiation schedule adopted here included measurements at 423 and 473°K before measurements at 223, 173 and 123°K, the latter three measurements were done on reverse-annealed cells. To adjust for this effect a set of measurements (numbers 6-9 in the sequence given in Table I) were made at 140 mW/cm^2 moving down in temperature after the 473° K measurement. By comparing these measurements with previous, pre-anneal, measurements at the same set of temperatures (numbers 1-4 in the Table I sequence) it was possible to adjust the low-temperature readings to the pre-anneal values. An illustration of the method used is shown in Figure 3 which gives plots of I_L

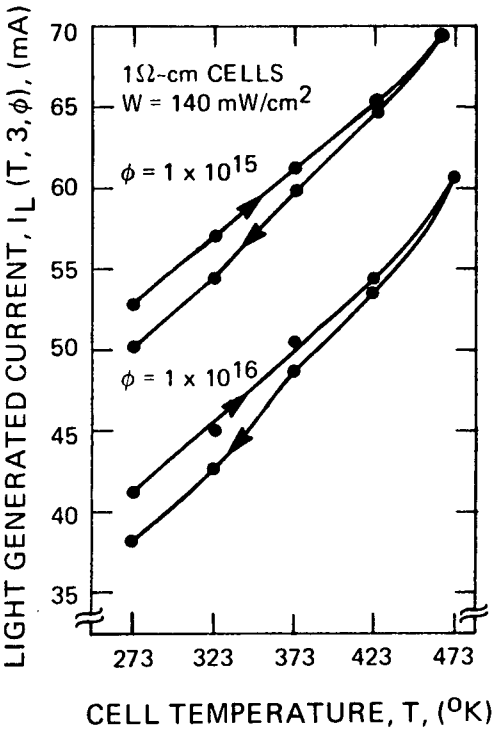

Figure 3. Light Generated Current Before and After 473°K Anneal

vs temperature before and after the reverse anneal. The plots are for 1 Ω-cm cells irradiated to 1×10^{15}e/cm^2 and 1×10^{16}e/cm^2. The curves with arrows pointing upward and to the right represent the pre-anneal measurements; those pointing downward and to the left, post-anneal measurements. Comparison of the curves shows that the reverse anneal has little effect on I_L at 423°K, that an increasing loss in I_L occurs between 373°K and 323°K, and that the loss is then approximately constant between 323°K and 273°K. These observations led to the choice of the fractional current loss at 273°K as the quantity to be added to the current values obtained in the low temperature measurements. Such an adjustment leads to an error less than the percentage of the adjustment. The highest adjustment was 8 percent (lower set of curves in Figure 3). All adjustments for fluences less than 1×10^{15}e/cm^2 were 2 percent or less for both resistivities; for fluences of 1×10^{15}e/cm^2 and greater the adjustments ranged from 2 to 3 percent for 10 Ω-cm cells and from 4-8 percent in 1 Ω-cm cells. Estimating that the percent error introduced by this adjustment is half of the percent adjustment, this error for fluences less than 1×10^{15} is ± 0.5 percent and for fluences of 1×10^{15}e/cm^2 and greater is ± 1 percent for 10 Ω-cm cells and ± 2 percent for 1 Ω-cm cells.

The maximum experimental error for a given T, W, ϕ and resistivity is the sum of all the errors discussed above. This sum (neglecting errors due to spectral mismatch and filters) varies from ± 1.4 percent for cells of either resistivity where W ≤ 140mW/cm^2, T ≥ 273°K, and $\phi < 1 \times 10^{15}$e/cm^2, to ± 3.6 percent for W > 140mW/cm^2, T < 273°K, $\phi \geq 1 \times 10^{15}$e/cm^2 and, 1 Ω-cm cell resistivity.

The spread in characteristics of a given group of cells places a basic limitation on the significance of predictions regardless of the accuracy of the measurements. An indication of the extent of cell current spread is given in Figure 4, which plots the results of pre-irradiation I_L measurements made on all 80 cells at T=273°K and W=140mW/cm^2. The number of cells with light-generated current greater than I_{LO} is plotted versus I_{LO} for 1 Ω-cm and 10 Ω-cm cells. The vertical bars on the curves mark the 10 percent great than — (or less than —) values, 80 percent of the cells being within these bars. The spread between bars is 4.3 percent for 10 Ω-cm cells and 4.7 percent for 1 Ω-cm cells. Results of post-irradiation measurements suggest that typical cell-to-cell variations at 5, 35, and 560mW/cm^2 illumination are approximately the same as those at 140mW/cm^2, but that variations at 1830mW/cm^2 are approximately twice as large. (A ten percent difference between high and low cell was common at 1830mW/cm^2 illumination.)

The average values of light generated current I_L, are given in Figure 4 for T=273°K, W=140mW/cm^2, and ϕ=0. The values are 69.5mA, and 68.6mA for 10 Ω-cm cells and 1 Ω-cm cells, respectively.

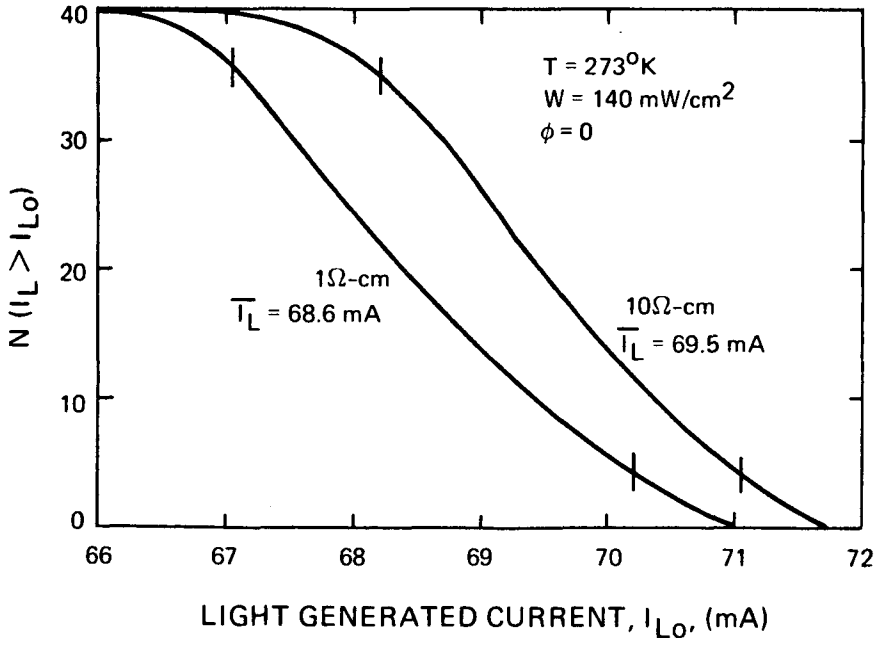

Figure 4. Distribution of Pre-Irradiation Values of Light Generated Current

2. Data and Empirical Equations

a. Fluence Dependence at 273°K, 140mW/cm^2

The analysis was initiated at the center of the temperature-illumination matrix, 273°K and 140mW/cm^2. Light generated current, I_L (4, 3, ϕ)* was plotted versus fluence and empirical fits were established. The data was first fitted to the customary logarithmic dependence; in the case of the 10 Ω-cm cells two separate equations were required for low and high fluence; for 1 Ω-cm cells one equation was used, but it included a fluence dependent multiplier having three separate fluence regions. The equations thus obtained are,

for 10 Ω-cm cells:

$$I_L\,(4,\ 3,\ \phi) = 127.2\ (1-0.0354\ \log_{10}\phi), \tag{1}$$

valid for $1 \times 10^{13} \leq \phi \leq 1 \times 10^{14}$e/cm^2, and

$$I_L\,(4,\ 3,\ \phi) = 197.2\ (1-0.0481\ \log_{10}\phi), \tag{2}$$

valid for $1 \times 10^{14} \leq \phi \leq 1 \times 10^{16}$e/cm^2;

for 1 Ω-cm cells:

$$I_L\,(4, 3,\ \phi) = 188.6\ \lambda_\phi\ (1-0.0481\ \log_{10}\phi), \tag{3}$$

where

$$\lambda_\phi = \begin{cases} 0.97 + 10^{-15}\ \phi, & \text{for } 1 \times 10^{13} \leq \phi \leq 3 \times 10^{13}\text{e/cm}^2 \\ 1.00, & \text{for } 3 \times 10^{13} \leq \phi \leq 3 \times 10^{15}\text{e/cm}^2 \\ 1.03 - 10^{-17}\ \phi, & \text{for } 3 \times 10^{15} \leq \phi \leq 1 \times 10^{16}\text{e/cm}^2. \end{cases}$$

An equally good fit to the experimental data, with a single equation valid over the entire fluence range, was obtained using a power law dependence of current on fluence. The appropriate equation was found by generating logarithmic plots of the quantity

$$\delta_I = \chi + I_L\,(4,\ 3,\ 1) - I_L\,(4,\ 3,\ \phi), \tag{4}$$

*The numbers and symbols in parentheses and all symbols used in this report are listed and explained in the glossary - Appendix A. Throughout this report I_L and V_O are given in milliamperes and volts, respectively.

versus fluence, ϕ, and by varying χ until the data fell along a straight line. Figure 5 shows the results of this method for both 10 Ω-cm and 1 Ω-cm cells. As seen in this figure, the experimental data for both resistivities fell along a straight-line with choices of χ = 13mA and χ = 15mA for 10 Ω-cm and 1 Ω-cm cells, respectively. These values of χ were also chosen to yield parallel lines, giving the same power law dependence for the two resistivities. This dependence was found to be

$$\delta_I = B_L \phi^{0.153}, \tag{5}$$

where B_L = 0.134 for 10 Ω-cm cells and 0.154 for 1 Ω-cm cells.

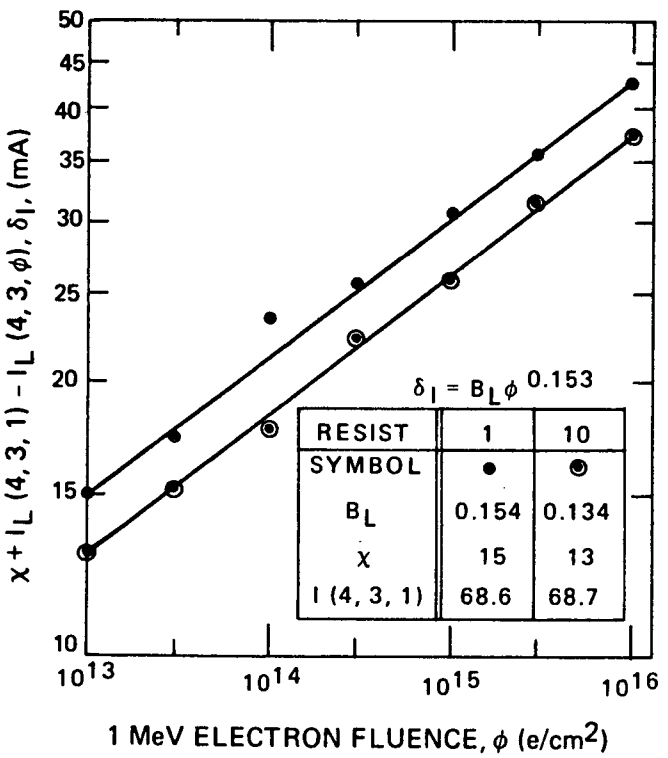

Figure 5. Fluence Dependence of the Parameter δ_I

The equations for I_L (4, 3, ϕ) were obtained by combining equations (4) and (5), inserting the appropriate values of χ and B_I, and inserting the experimental values of I_L (4, 3, 1), the current at $\phi = 1 \times 10^{13} e/cm^2$. These values were 68.7mA and 68.6mA, respectively for 10 Ω-cm and 1 Ω-cm cells* giving the equations,

for 10 Ω-cm cells:

$$I_L (4, 3, \phi) = 81.7 - 0.134 \phi^{0.153}, \quad (6)$$

for 1 Ω-cm cells:

$$I_L (4, 3, \phi) = 83.6 - 0.154 \phi^{0.153}, \quad (7)$$

both of which are valid over the entire fluence range:

$$1 \times 10^{13} \leq \phi \leq 1 \times 10^{16} e/cm^2.$$

Figures 6 and 7 give plots of I_L (4, 3, ϕ) versus fluence for 10 Ω-cm cells and 1 Ω-cm cells, respectively. The experimental data points, the logarithmic equations, and the power-law equation are all shown. It is seen that both equations fit the data well except for one large deviation, this being at $\phi = 1 \times 10^{14} e/cm^2$ in Figure 7. The deviation from this data point is 2.5 percent for the logarithmic equation and 3.6 percent for the power-law equation. However, the cells represented by this data point are themselves suspect since they behaved oppositely to all of the other cell groups during exposure to high temperature, showing an increase rather than a decrease in current after the high temperature measurements. (The reason for this is not understood, but our guess is that these cells might have been heated to a higher temperature than the others during solder-mounting on the cell block.) It was therefore concluded that a quirk in the cells was responsible for this large deviation.

b. Temperature Coefficient

The temperature dependence of I_L under 140mW/cm^2 illumination was next considered. For temperatures of 273°K and above the light-generated current varied approximately linearly with temperature with a temperature coefficient that increased with increasing fluence. It was discovered that the

*The difference of 0.1mA between resistivities contrasts with the 0.9mA difference in overall average between 1 and 10 Ω-cm unirradiated cells. This resulted because of a 0.9mA lower-than average pre-irradiation current in the 10 Ω-cm cells irradiated to $1 \times 10^{13} e/cm^2$. The equation for the 10 Ω-cm cells is therefore probably conservative at this fluence.

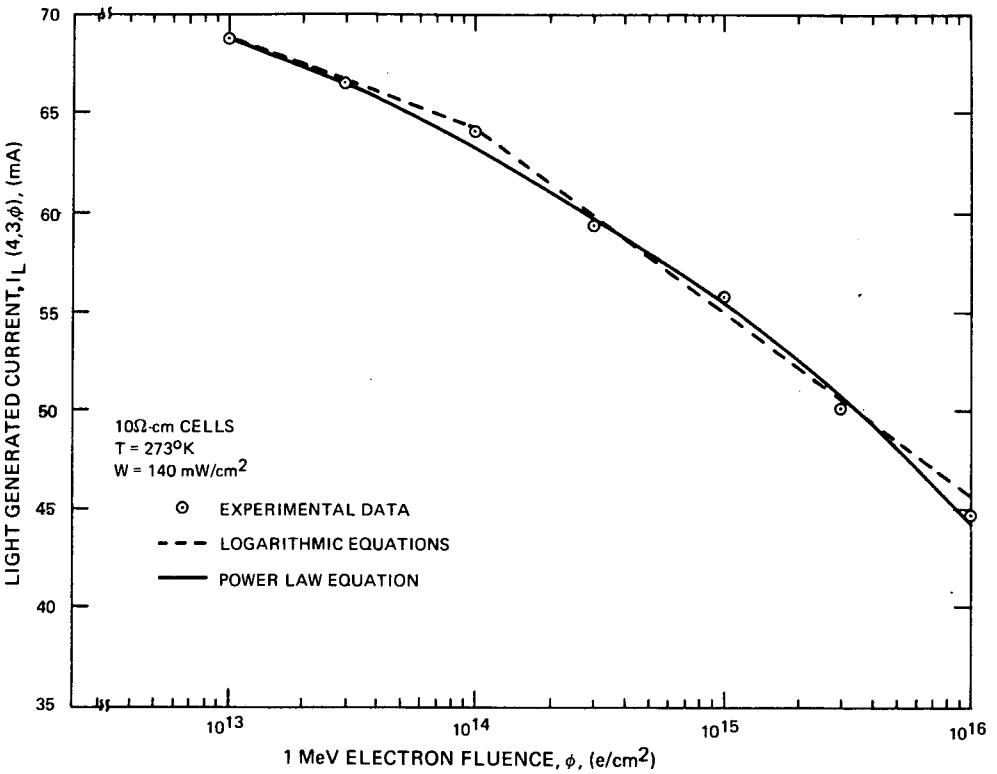

Figure 6. Light Generated Current vs Fluence at 273°K and 140 mW/cm^2 Illumination, 10Ω-cm Cells

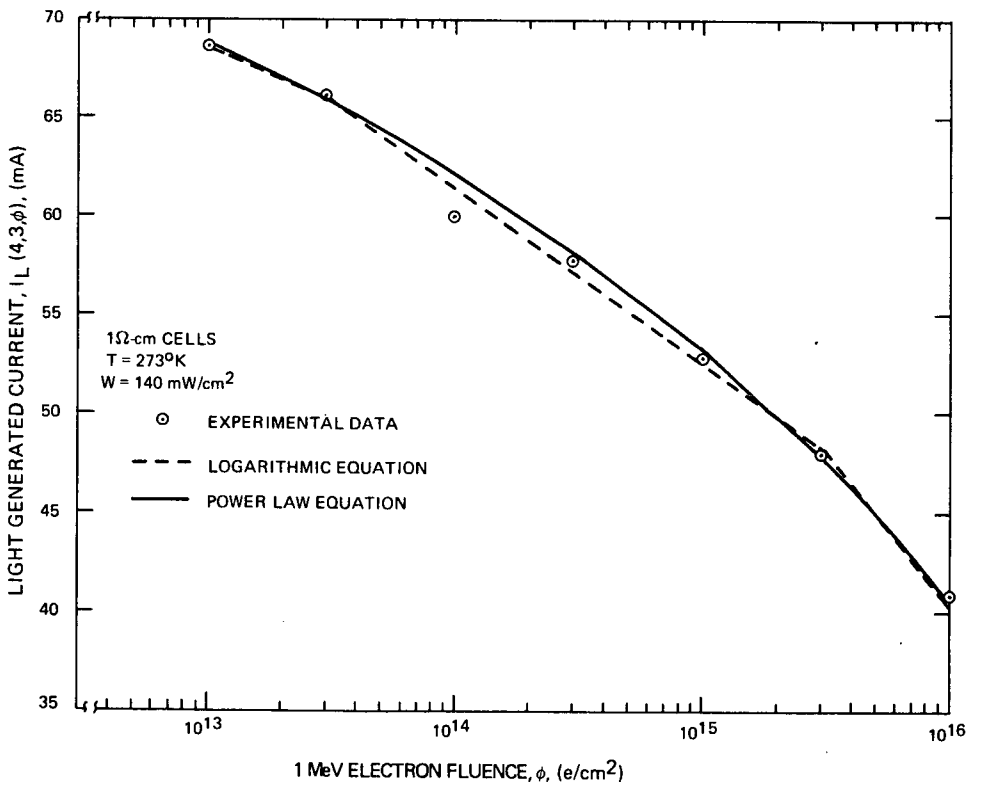

Figure 7. Light Generated Current vs Fluence at 273°K and 140 mW/cm^2 Illumination, 1 Ω-cm Cells

temperature coefficient, dI_L/dT, divided by the current at 273°K, I_L (4, 3, ϕ), followed a power law relationship with fluence. This relationship is seen in Figure 8 which gives plots of normalized temperature coefficient versus fluence. Both 10 Ω-cm and 1 Ω-cm cell data are fitted to a good approximation by the relationship,

$$\frac{1}{I_L\,(4,3,\phi)}\,\frac{dI_L}{dT} = 3.23\times 10^{-6}\,\phi^{\,0.18}, \qquad (8)$$

over the entire fluence range.

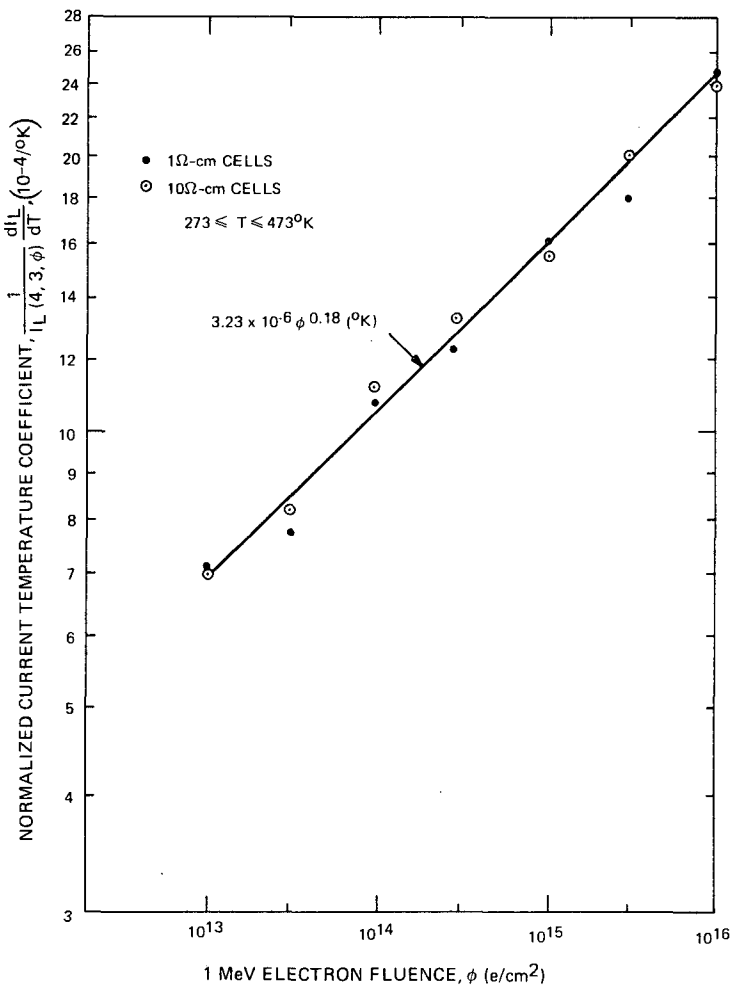

Figure 8. Normalized Temperature Coefficient of Light Generated Current Versus Fluence

At temperatures below approximately 223°K the behavior was different, the temperature coefficient being relatively independent of fluence. This was particularly true for the 10 Ω-cm cells where dI_L/dT averaged 0.055mA/°K over the range of fluences. For 1 Ω-cm cells a slight fluence dependence was apparent, but a large scatter in the data prompted the use of the value averaged over all fluences, which was 0.062mA/°K.

c. Fluence and Temperature Dependence at 140mW/cm^2

Combining the temperature and fluence dependencies developed above, equations can be written for the light-generated current valid for all temperatures and fluences covered in the experiment. The current is given by

$$I_L\,(T,\ 3,\ \phi) = I_L\,(4,\ 3,\ \phi)\left[1 + \frac{1}{I_L\,(4,\ 3,\ \phi)}\,\frac{dI_L}{dT}\,(T-273)\right]. \qquad (9)$$

Combining equations (6)*, (7)*, (8) and (9), the light generated current equations are,

for 10 Ω-cm cells, for T ≥ 223°K:

$$I_L\,(T,\ 3,\ \phi) = \left(81.7-0.134\,\phi^{\,0.153}\right)\left[1 + 3.23\times10^{-6}\,\phi^{\,0.18}\,(T-273)\right], \qquad (10)$$

and for T ≤ 223°K:

$$I_L\,(T,\ 3,\ \phi) = I\,(3,\ 3,\ \phi) + 0.055\,(T-223), \qquad (11)$$

where I (3, 3, φ) is obtained from equation (10);

for 1 Ω-cm cells, for T ≥ 273°K

$$I_L\,(T,\ 3,\ \phi) = \left(83.6 - 0.154\,\phi^{\,0.153}\right)\left[1 + 3.23\times10^{-6}\,\phi^{\,0.18}\,(T-273)\right], \qquad (12)$$

and for T ≤ 273°K:

$$I_L\,(T,\ 3,\ \phi) = 83.6 - 0.154\,\phi^{\,0.153} + 0.062\,(T-273). \qquad (13)$$

Note that equation (10), the high temperature equation for 10 Ω-cm cells extends to a lower temperature than its counterpart for 1 Ω-cm cells, equation (12). As a consequence the low temperature equation (11) is based on I_L (3, 3, φ), the current 223°K, rather than I_L (4, 3, φ), the current at 273°K.

Figures 9 through 12 give plots of light generated current versus cell temperature with fluence as a parameter. Both the experimental data and the curves

*The power-law fluence relationships will be used hereafter.

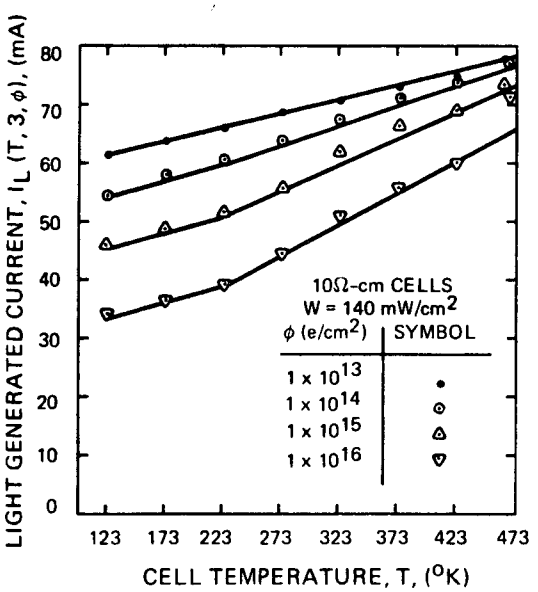

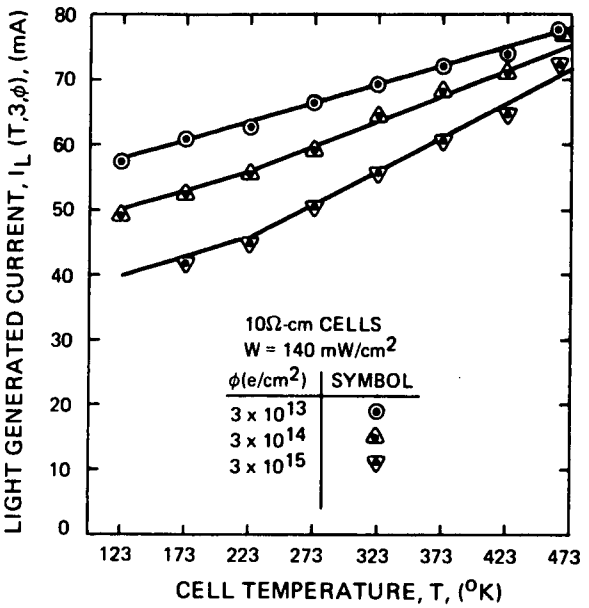

Figures 9 and 10. Light Generated Current at W = 140 mW/ cm² Versus Cell Temperature and Fluence, 10Ω-cm Cells

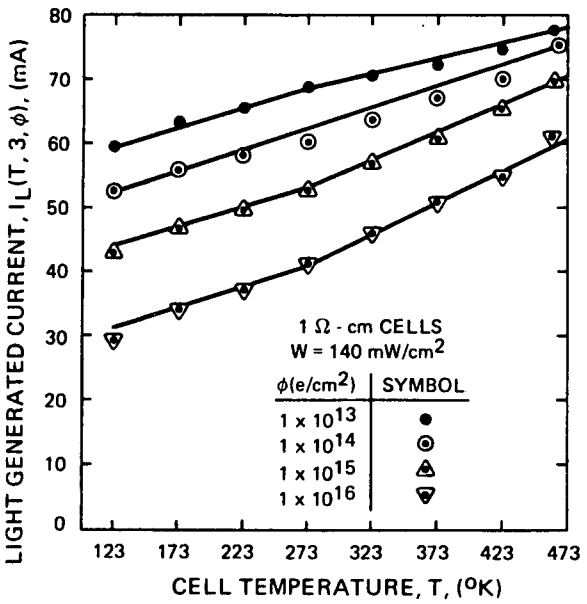

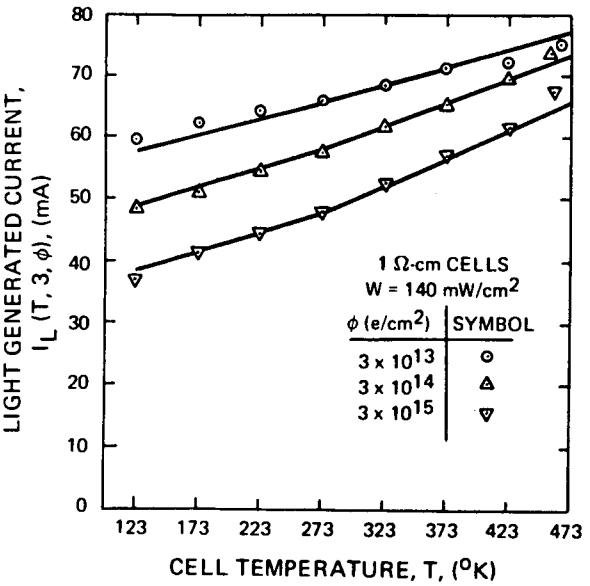

Figures 11 and 12. Light Generated Current at W = 140 mW/ cm² Versus Cell Temperature and Fluence, 1Ω-cm Cells

representing the appropriate equations are shown, Figures 9 and 10 representing 10 Ω-cm cells and equations (10) and (11); Figures 11 and 12 representing 1 Ω-cm cells and equations (12) and (13). The several characteristics which the two resistivities have in common are clear from the data and the similarities in their empirical equations. Another, which shows up in the Figures, is the match between high and low temperature coefficients at low fluence, i.e., the linearity of I_L vs T over the entire temperature range. However, several subtle but significant differences are in evidence. First, as noted above, the high temperature equation for the 10 Ω-cm cells extends down to 223°K, 50°K further than its counterpart for 1 Ω-cm cells. This, of course, was dictated by the experimental data, which shows the fluence dependent temperature coefficient for the 10 Ω-cm cells to extend down to 223°K. Secondly, although there is an obvious break in the curves for $\phi \geq 3 \times 10^{14} e/cm^2$ for both resistivities, the break is significantly stronger for the 10 Ω-cm cells, their temperature coefficient being lower at low temperature and higher at high temperature than that for the 1 Ω-cm cells. (The normalized temperature coefficients, equation (8) are the same for both resistivities at high temperature, but the normalizing currents are lower for the 1 Ω-cm cells. Consequently the absolute coefficients are higher for the 10 Ω-cm cells.)

It is evident from Figures 9-12 that the quality of the empirical fit to the data is good except for a few isolated points. A detailed discussion of the empirical fits at all illuminations is given in part f of this section.

d. Fluence and Temperature Dependence at 5 and 35mW/cm^2

In deriving empirical equations for illumination intensities other than 140mW/cm^2, the initial approach assumed the fluence and temperature dependencies obtained at 140mW/cm^2 and a linear dependence of current on illumination, i.e.,

$$I_L(T, W, \phi) = \frac{W}{140} \left[I_L(T, 3, \phi) \right], \qquad (14)$$

where $I_L(T, 3, \phi)$ is obtained from the appropriate number among equations (10) - (13). The results of this approach are illustrated in Figures 13 - 15.

Figure 13 gives plots of equation (14) and the experimental values of current at 35mW/cm^2 illumination versus cell temperature at four fluences for 10 Ω-cm cells. The equation provides a good fit to the data, in particular, predicting the break in the slope (temperature coefficient) which is in evidence in the data. Corresponding plots for 1 Ω-cm cells are given in Figure 14. Again, a reasonably good fit is obtained, however the break in the slope is not in evidence in the data. Since no data was taken at 35mW/cm^2 above 323°K, (50°K above the break for 1 Ω-cm cells at 140mW/cm^2 illumination) it is not possible to ascertain from the present data whether or not this break is actually absent in the 1 Ω-cm cells.

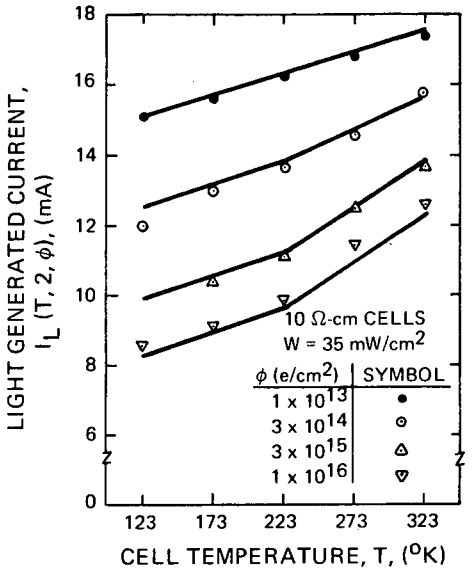

Figure 13. Light Generated Current at W = 35 mW/ cm^2 Versus Cell Temperature and Fluence, 10 Ω-cm Cells

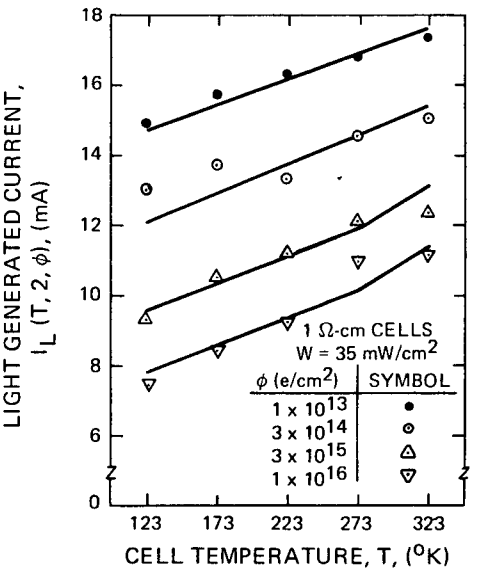

Figure 14. Light Generated Current at W = 35 mW/ cm^2 Versus Cell Temperature and Fluence, 1 Ω-cm Cells

Figure 15 gives plots of equation (14) and the experimental data at 5mW/cm^2 illumination for both 10 Ω-cm and 1 Ω-cm cells. All of the data at this illumination are at 223°K and below so equations (11) and (13), the low-temperature equations which give fluence-independent temperature coefficients, apply. This fluence-independence is reflected in the data for cells of both resistivities.

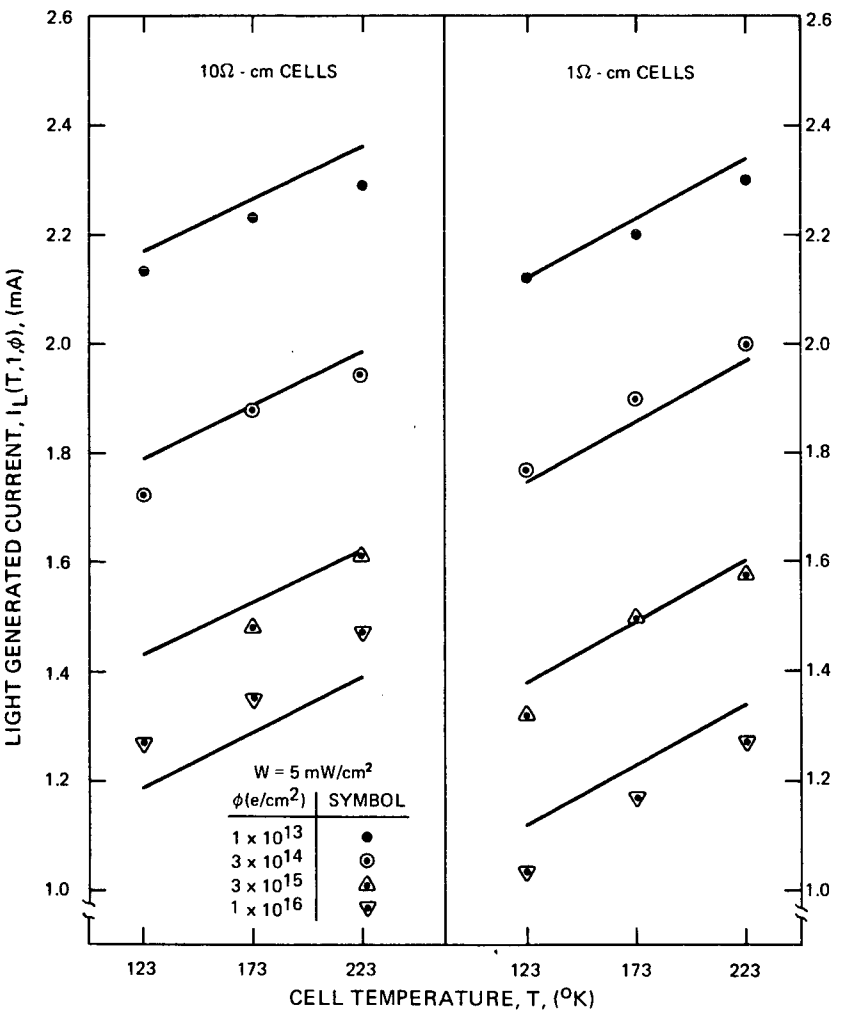

Figure 15. Light Generated Current at W = 5 mW/ cm^2 Versus Cell Temperature and Fluence, 10 Ω-cm and 1 Ω-cm Cells

e. Fluence and Temperature Dependence at 560 and 1830mW/cm^2

Equation (14) did not accurately predict the light-generated current at 560mW/cm^2 and a modified version was adopted:

$$I_L (T, W, \phi) = \xi_W \left[I_L (T, 3, \phi) \right], \qquad (15)$$

where ξ_W is an illumination-dependent coefficient determined separately for each cell resistivity but is independent of fluence and cell temperature. Equation (15) drops the assumption of a linear current-illumination relationship but maintains the temperature and fluence relationships derived for 140mW/cm^2 illumination.

The results for 560mW/cm^2 illumination are shown in Figures 16 and 17 for 10Ω-cm cells, and 1Ω-cm cells, respectively. The criterion for the best-fit value of ξ_W was that the deviation between the equation and the data averaged over the 35 data points be zero. This resulted in values for ξ_W of 3.66 and 3.63 for 10 Ω-cm cells and 1 Ω-cm cells, respectively. These values are approximately 9 percent below the value of 4.0 for W/140. The reason for this apparent divergence from linearity is not known. However, it is felt that a calibration error due to uncertainties in neutral-density filter transmission may be responsible.

As indicated in Figures 16 and 17, equation (15) provides an acceptable fit to the data using the appropriate values of ξ_W, thus the same general temperature fluence dependencies apply to this illumination as did at 140mW/cm^2. Since the 560mW/cm^2 data are at 273°K and above, equations (10) and (12), the high temperature equations predicting an increase in temperature coefficient with fluence, apply. This dependence is accurately reflected in the data for both 10 Ω-cm and 1 Ω-cm cells.

Figure 18 shows current versus temperature plots at four fluences for both 10 Ω-cm and 1 Ω-cm cells for the illumination intensity of 1830mW/cm^2. The curves were obtained using equation (15) with ξ_W values of 12.86 and 12.50 for 10 Ω-cm cells and 1 Ω-cm cells, respectively. These values are within 5 percent of the value of 13.1 for W/140. Considering the experimental error of up to ± 4 percent and cell-to-cell variations of up to 10 percent this difference is not considered significant. The equations give adequate predictions of fluence dependence, and the predicted increase in temperature coefficient with fluence is in evidence in the data. However, given the high degree of scatter in the experimental results, the criteria for an equation describing them are rather modest, i.e., (1) a reasonably good general fit and (2) a form proven valid in other experiments with a better data base. Equation (15) satisfies both of these criteria, but a better data base is required to test its accuracy.

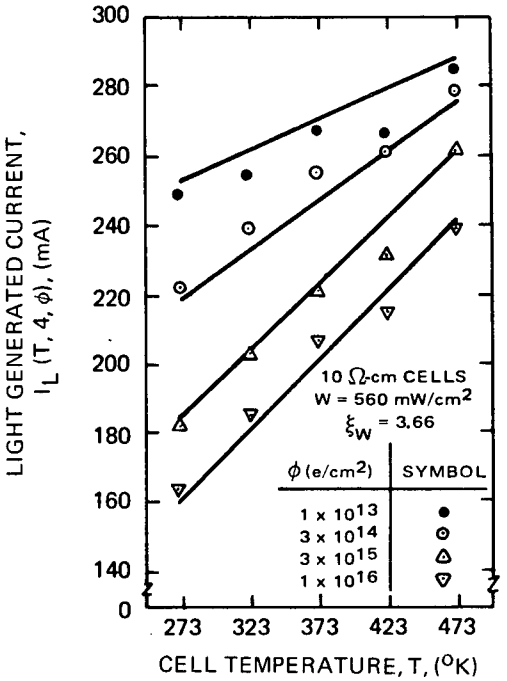

Figure 16. Light Generated Current at W = 560 mW/ cm^2 Versus Cell Temperature and Fluence, 10 Ω-cm Cells

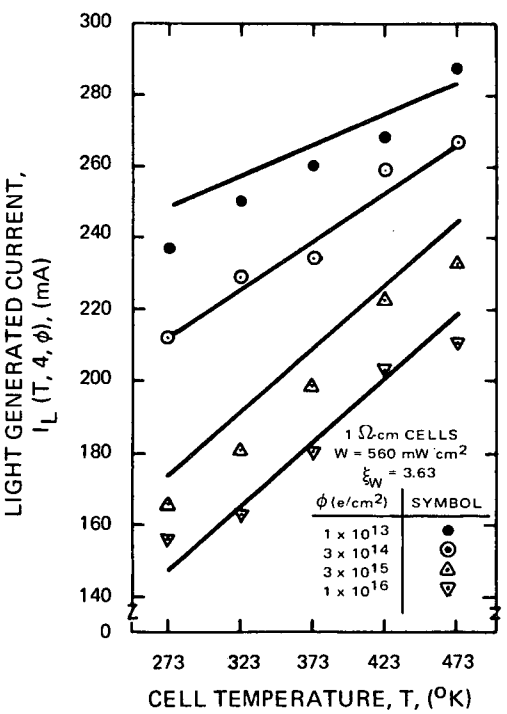

Figure 17. Light Generated Current at W = 560 mW/ cm^2 Versus Cell Temperature and Fluence, 1 Ω-cm Cells

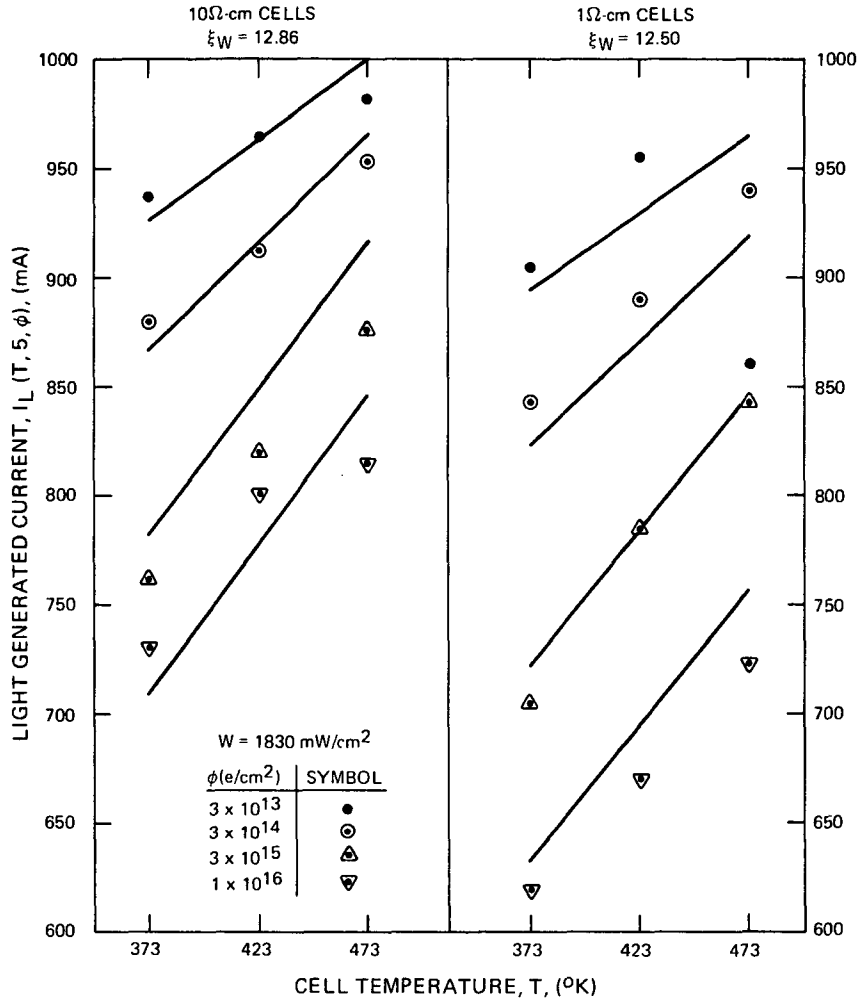

Figure 18. Light Generated Current at W = 1830 mW/ cm^2 Versus Cell Temperature and Fluence, 10 Ω-cm, and 1 Ω-cm Cells

f. Quality of Empirical Fit

An indication of the quality of the empirical fit to the data was obtained by computing the percent deviation, E, given by

$$E = 100 \frac{(I_D - I_E)}{(I_D + I_E)/2}, \tag{16}$$

where I_D and I_E are the values of light generated current obtained from the experimental data and from the appropriate empirical equation, respectively.

This quantity was computed for each data point. Since data was taken at each of seven fluences and eight temperatures at 140mW/cm^2, five temperatures at 35 and 560mW/cm^2, and three temperatures at 5 and 1830mW/cm^2, the nominal number* of data points for each resistivity were 56, 35, 35, 21, and 21, for 140mW/cm^2, 35mW/cm^2, 560mW/cm^2, 5mW/cm^2 and 1830mW/cm^2, respectively.

In Figure 19, the number of readings with absolute value of E greater than E_o, N ($|E| > |E_o|$), is plotted versus E_o for each of the five illuminations for 10 Ω-cm cells. (E_o is plotted on both sides of the origin to accommodate the five curves.) All but 3 of the 55 points for W=140mW/cm^2 show a deviation between data and equation of less than three precent, only one point shows a deviation greater than 4 percent. Thus the equation provides a good fit to all but this single data point, the point at $\phi = 1 \times 10^{16}$e/cm^2, T = 473°K, which is 8.3 percent higher than the equation predicts. Examination of Figures 9 and 10 shows an upturn in data at 473°K at other fluences as well as at 1×10^{16}e/cm^2 suggesting a greater than linear increase in current at very high temperatures.** Close examination of the data (Figures 9-12) indicates the possibility of further complexities in temperature dependence. Such complexities have been previously reported[11] however the equations derived here are believed to be adequate given the experimental accuracy of the present results.

At other illuminations the number of points representing greater than 4 percent deviation are:

3 of 34 points for 35mW/cm^2,

5 of 35 points for 560mW/cm^2,

5 of 20 points for 5mW/cm^2,

4 of 20 points for 1830mW/cm^2.

From the above and Figure 19, the quality of the fit is best at 140mW/cm^2, and is worst at the ends of the illumination matrix, i.e., at 5 and 1830mW/cm^2. However, at all intensities, at least 80 percent of the data points are within

*There are fewer in some cases due to missed readings at 123°K.

**The same comments apply to 1 Ω-cm cells, see Figures 11 and 12.

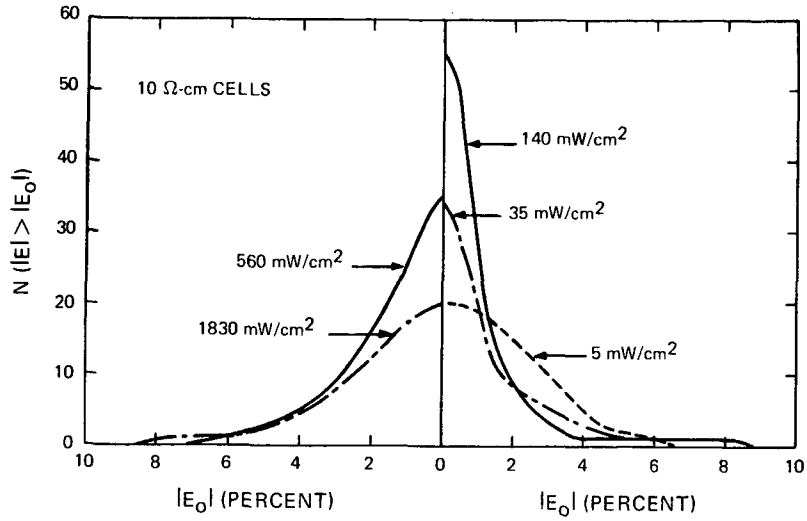

Figure 19. Divergence of I_L Values of Empirical Equations from Experimental I_L Values, 10 Ω-cm Cells

4 percent of the value calculated from the appropriate equation. The fit for 10 Ω-cm cells is thus considered adequate at all intensities.

Similar plots of $N(|E| > |E_0|)$ versus E_0 are given for 1 Ω-cm cells in Figure 20. The number of points representing greater than 4 percent deviation are:

3 of 56 points for 140mW/cm^2,

4 fo 35 points for 35mW/cm^2,

7 of 34 points for 560mW/cm^2,

7 of 21 points for 5mW/cm^2,

3 of 19 points for 1830mW/cm^2.

Comparison of Figures 19 and 20 show the fit for 10 Ω-cm cells to be slightly better than that for 1 Ω-cm cells. This is not unexpected since cell-to-cell variations and the error introduced by the high temperature reverse anneal are smaller in the 10 Ω-cm cells.

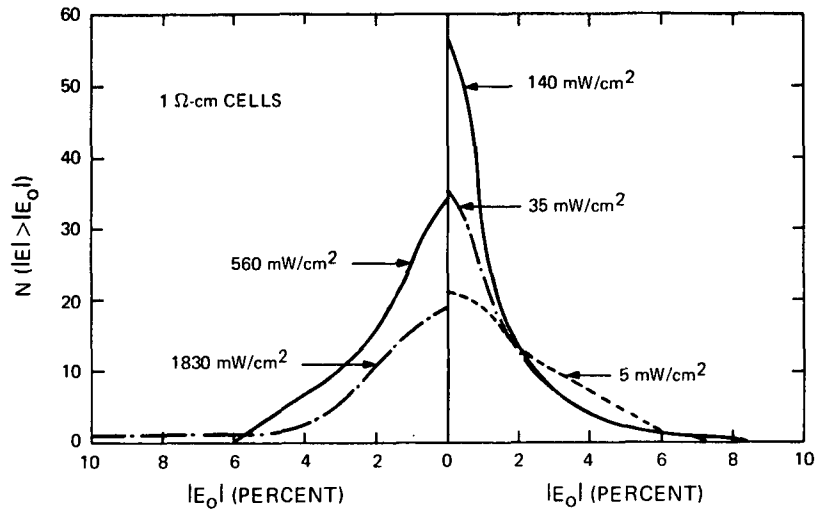

Figure 20. Divergence of I_L Values of Empirical Equations from Experimental I_L Values, 1 Ω-cm Cells

C. OPEN CIRCUIT VOLTAGE

1. Measurement Uncertainties

The experimental error in open circuit voltage due to illumination-intensity variations is small because of the relative insensitivity of V_O to intensity. Equations derived below show that the difference in open-circuit voltage, ΔV_O, for two different intensities, W_1 and W_2 is given by $\Delta V_O = 0.025 \ln (W_2/W_1)$ for 10 Ω-cm cells and $\Delta V_O = 0.032 \ln (W_2/W_1)$ for 1 Ω-cm cells. Thus a 3 percent intensity variation results in an error in V_O of less than 0.001V.

The largest source of experimental error results from the temperature uncertainty of ± 3°K. Open-circuit-voltage temperature coefficients were found to be approximately -0.0023 V/°K. Consequently the temperature uncertainty leads to a V_O uncertainty of ± 0.007V.

Cell-to-cell variations must also be considered. Figure 21 shows results of pre-irradiation measurements of open circuit voltage taken at 273°K and 140mW/cm^2 illumination. The number of cells with open circuit voltage greater than V_{OO}, N ($V_O > V_{OO}$), is plotted versus V_{OO} for 10 Ω-cm and 1 Ω-cm cells. The group averages are 0.615V and 0.647V respectively. For both resistivities 80 percent of the cells lie within ± 0.010V of the average values. The extent of cell-to-cell variations is thus comparable to the error introduced by the tem-

perature uncertainty and therefore indistinguishable from it. Accordingly the combined uncertainty in the measurement of V_o is estimated to be approximately ±0.012V. Since this uncertainty is essentially constant over the measurement temperature range, the percent error increases with temperature (since V_o decreases with increasing temperature).

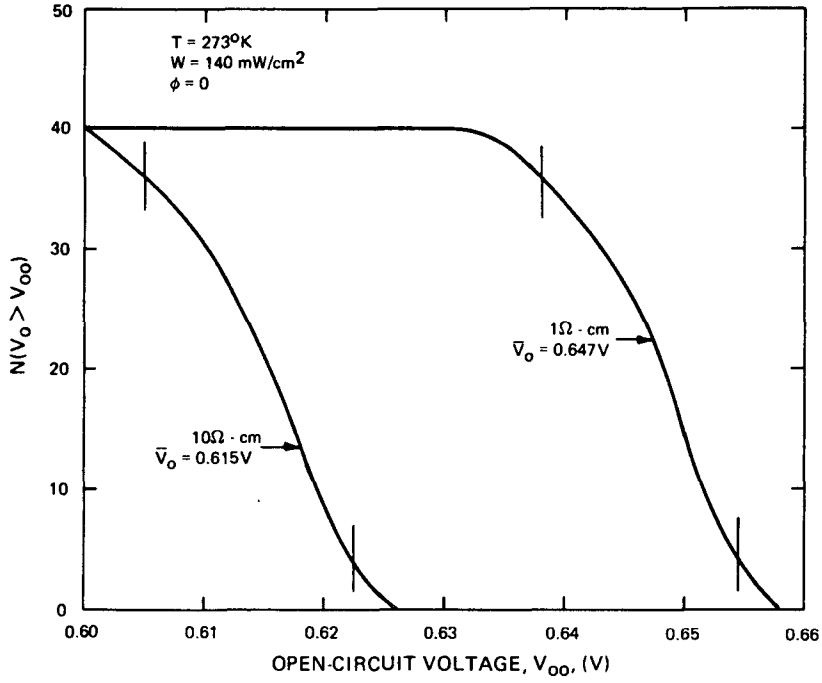

Figure 21. Distribution of Pre-Irradiation Values of Open Circuit Voltage

2. Data and Empirical Equations

a. Fluence Dependence

In a manner similar to that employed in the analysis of light-generated current, power-law expressions were derived relating V_o at 273°K and 140mW/cm² illumination to fluence.

The quantity

$$\delta_V = \chi + V_o(4, 3, 1) - V_o(4, 3, \phi) \quad (17)$$

is plotted versus fluence in Figure 22. By choosing values of χ equal to 0.013V and 0.017V for 10 Ω-cm cells and 1 Ω-cm cells, respectively, it was possible to fit the data of both resistivities to the same equation, namely

$$\delta_V = 9.35 \times 10^{-6} \phi^{0.25}. \quad (18)$$

By combining equations (17) and (18) and inserting the experimental values for V_o (4, 3, 1), i.e., 0.608V for 10 Ω-cm cells, and 0.634V for 1 Ω-cm cells, expressions for V (4, 3, ϕ) were obtained which are valid for $1 \times 10^{13} \leq \phi \leq 1 \times 10^{16} e/cm^2$,

for 10 Ω-cm cells:

$$V_o (4, 3, \phi) = 0.621 - 9.35 \times 10^{-6} \phi^{0.25}, \quad (19)$$

for 1 Ω-cm cells:

$$V_o (4, 3, \phi) = 0.651 - 9.35 \times 10^{-6} \phi^{0.25}. \quad (20)$$

In Figure 22 all but one data point is within 0.005V of the curve representing equations (19) and (20). The exception is the point for 1 Ω-cm cells irradiated to $1 \times 10^{14} e/cm^2$, the cell group previously noted as suspect due to its unusual behavior at high temperature.

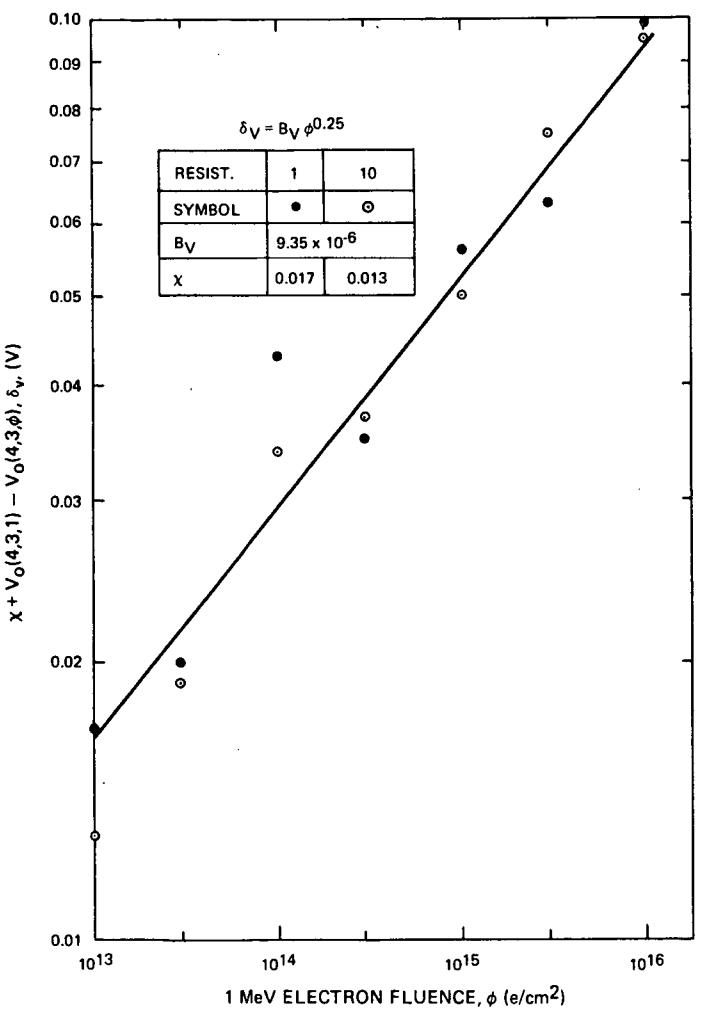

Figure 22. Fluence Dependence of the Parameter δ_V

b. Temperature and Illumination Dependence

Plots of V_o versus cell temperature are given for 10 Ω-cm cells in Figures 23 to 26. Each figure gives values for the five intensities of illumination, covering the temperature range from 223°K to 473°K. Each represents a different fluence, 1×10^{13}, 3×10^{14}, 3×10^{15}, and $1 \times 10^{16} e/cm^2$ being shown in Figures 23, 24, 25, and 26, respectively. The data at all illuminations and fluences within this temperature range have been fitted by the single equation,

$$V_o(T, W, \phi) = 0.621 - 9.35 \times 10^{-6} \phi^{0.25} - 0.0023 (T - 273) + 0.025 \ln \left(\frac{W}{140}\right). \quad (21)$$

Equation (21), which is also plotted in Figures 23 to 26, is equation (19) with terms added for temperature and illumination dependence. The temperature-dependent term indicates a temperature coefficient of 0.0023V/°K which is constant independent of fluence, cell temperature, and illumination. The illumination dependent term indicates a constant voltage difference between two different illuminations, independent of temperature and fluence.

Plots of V_o versus cell temperature for 1 Ω-cm cells are given in Figures 27, 28, 29, and 30, for fluences of 1×10^{13}, 3×10^{14}, 3×10^{15}, and $1 \times 10^{16} e/cm^2$, respectively. (No data at $5 mW/cm^2$ is presented since V_o at this illumination was degraded by a high empirical A factor - see section IIE. 2.) The equation derived to fit the data is

$$V_o(T, W, \phi) = 0.651 - 9.35 \times 10^{-6} \phi^{0.25} - C_T (T-273) + 0.032 \ln \left(\frac{W}{140}\right), \quad (22)$$

where $C_T = 0.0022 V/°K$ for $1 \times 10^{13} \leq \phi \leq 1 \times 10^{14} e/cm^2$, and $0.0023 V/°K$ for $3 \times 10^{14} \leq \phi \leq 1 \times 10^{16} e/cm^2$. In contrast to the 10 Ω-cm cells the temperature coefficient for 1 Ω-cm cells has a significant fluence dependence as described by these two different values of C_T. In addition, the coefficient of the illumination-dependent term is larger for the 1 Ω-cm cells. Otherwise the equations are very similar; in particular for $W=140 mW/cm^2$ and $\phi \geq 3 \times 10^{14} e/cm^2$ the difference in open-circuit voltage between the two resistivities is constant at 0.030V.

An interesting feature in the data for both resistivities is the approximate parallelism in the curves at different illuminations, reflected in the illumination-dependent terms of equations (21) and (22). The current-voltage (I-V) equation for a solar cell having series resistance, R_S, is

$$I = I_L - I_F = I_L - I_o \left[\exp\left(\frac{eV}{AkT} + IR_s\right) - 1 \right], \quad (23)$$

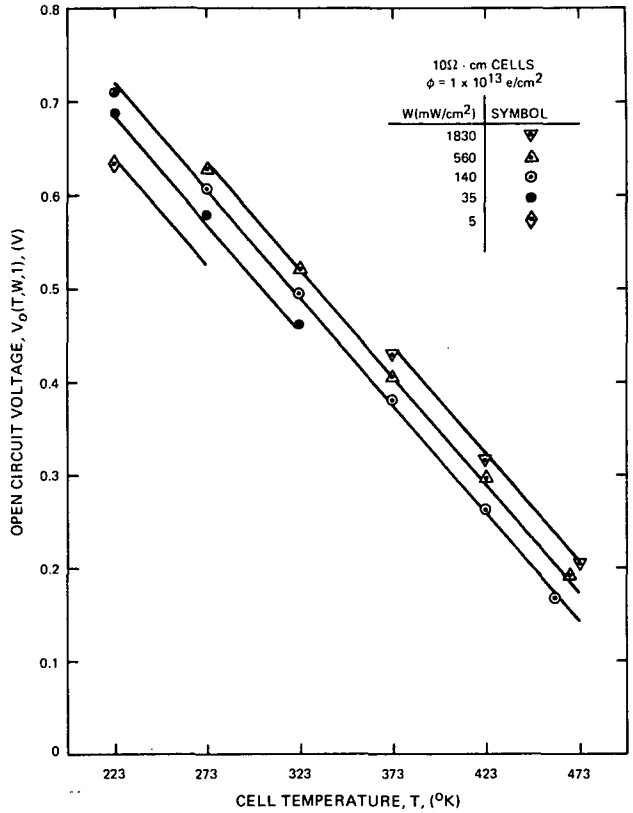

Figure 23. Open Circuit Voltage Versus Cell Temperature and Illumination at $\phi = 1 \times 10^{13} e/cm^2$, 10 Ω-cm Cells

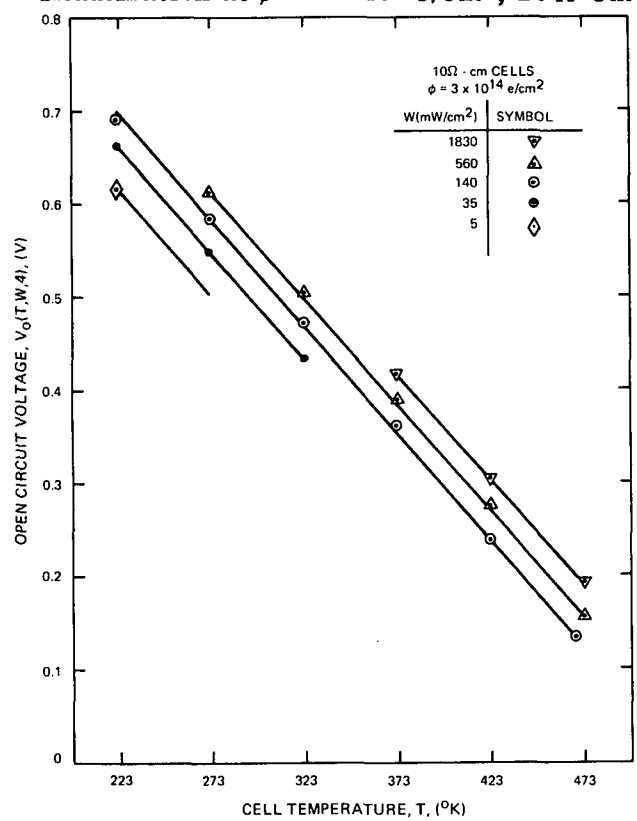

Figure 24. Open Circuit Voltage Versus Cell Temperature and Illumination at $\phi = 3 \times 10^{14} e/cm^2$, 10 Ω-cm Cells

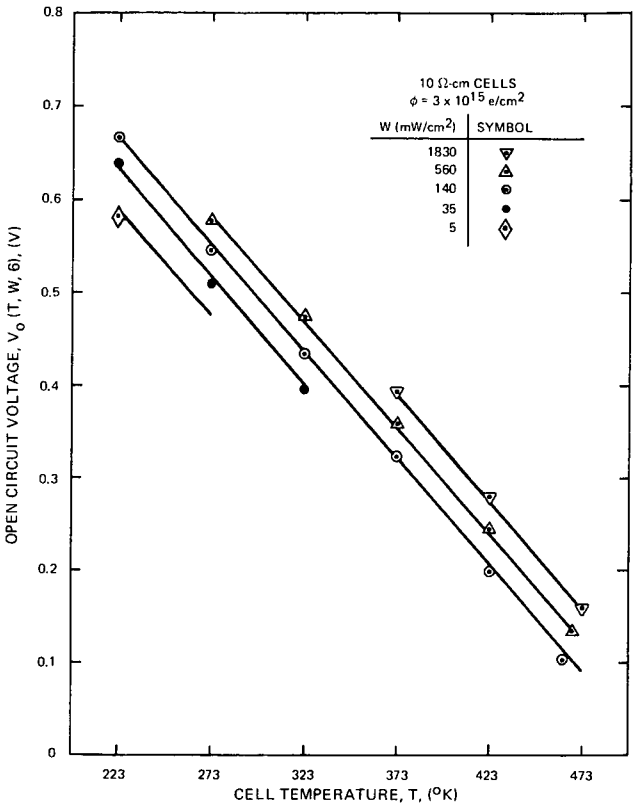

Figure 25. Open Circuit Voltage Versus Cell Temperature and Illumination at $\phi = 3 \times 10^{15}$e/cm^2, 10 Ω-cm Cells

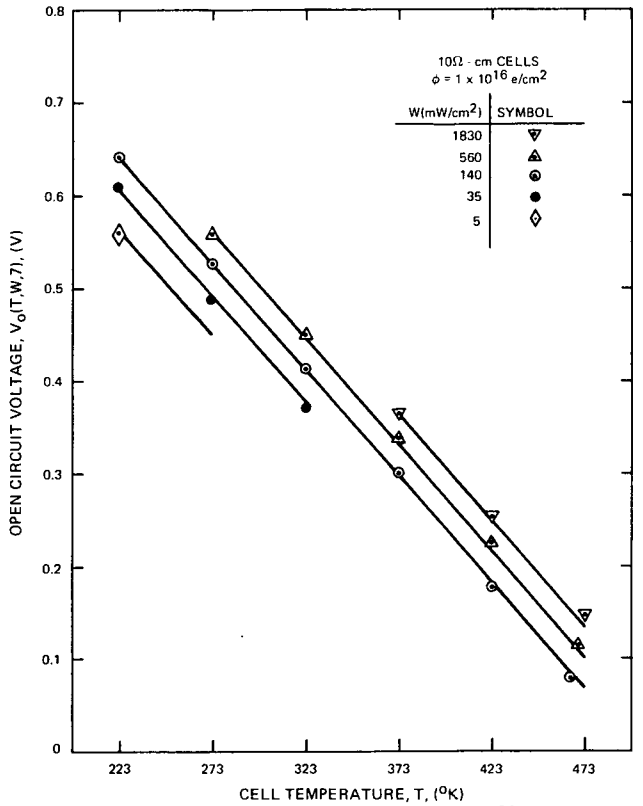

Figure 26. Open Circuit Voltage Versus Cell Temperature and Illumination at $\phi = 1 \times 10^{16}$e/cm^2, 10 Ω-cm Cells

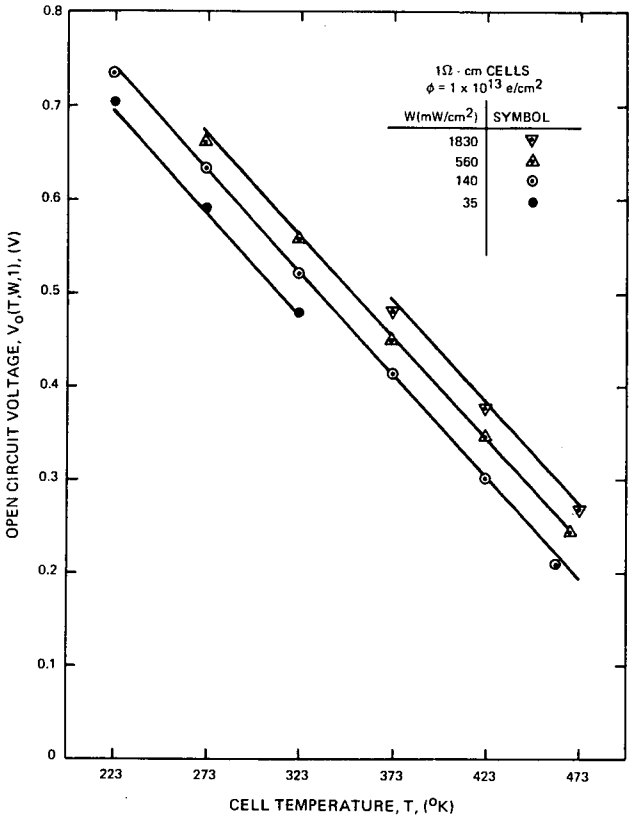

Figure 27. Open Circuit Voltage Versus Cell Temperature and Illumination at $\phi = 1 \times 10^{13}$e/cm^2, 1 Ω-cm Cells

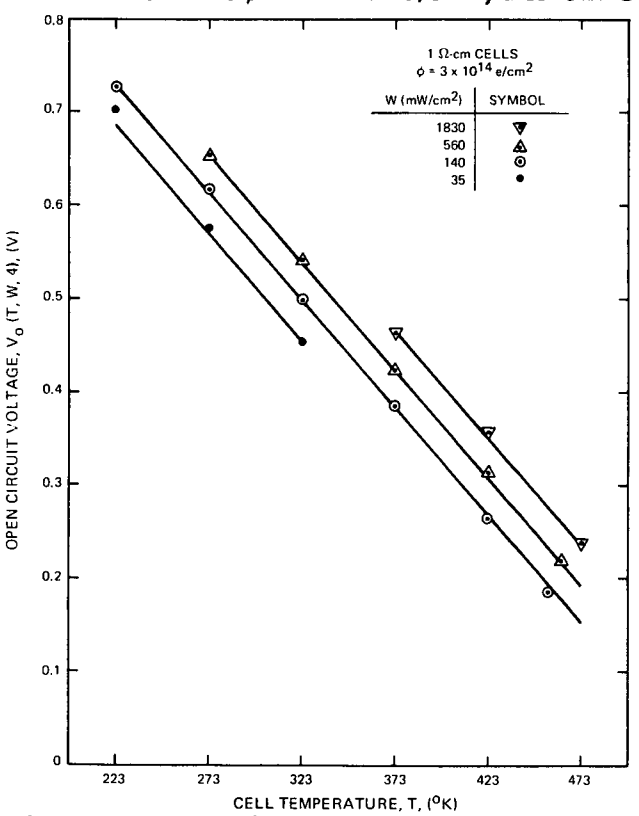

Figure 28. Open Circuit Voltage Versus Cell Temperature and Illumination at $\phi = 3 \times 10^{14}$e/cm^2, 1 Ω-cm Cells

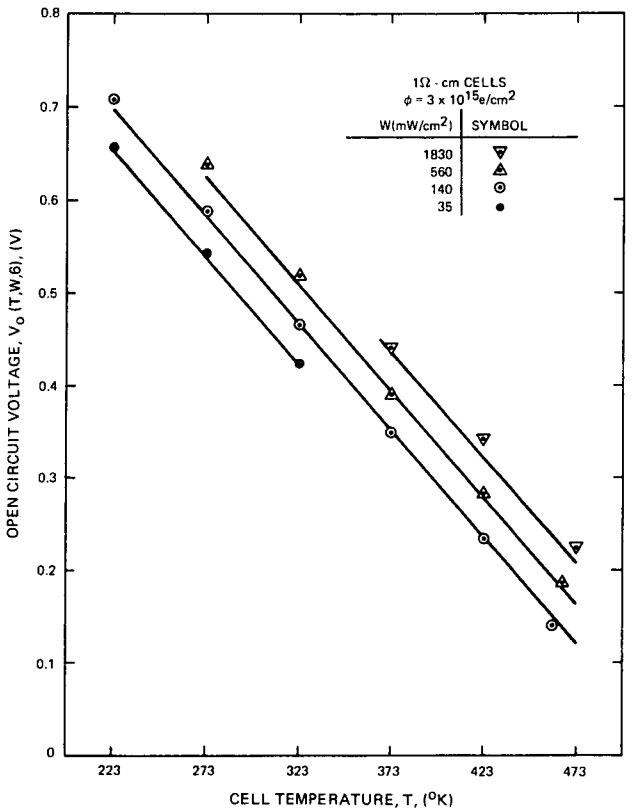

Figure 29. Open Circuit Voltage Versus Cell Temperature and Illumination at $\phi = 3 \times 10^{15} e/cm^2$, 1 Ω-cm^{2}Cells

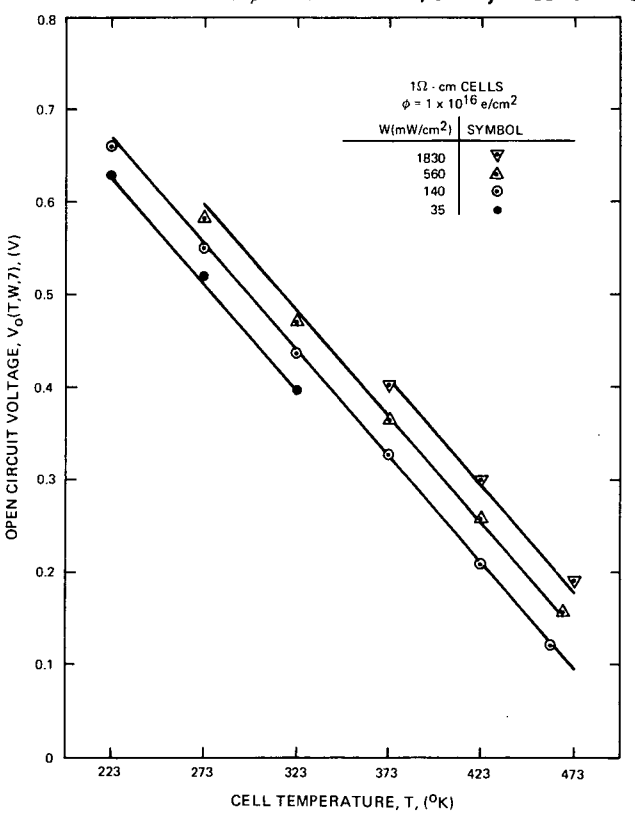

Figure 30. Open Circuit Voltage Versus Cell Temperature and Illumination at $\phi = 1 \times 10^{16} e/cm^2$, 1 Ω-cm Cells

where the symbols used are defined in Appendix A. Open circuit voltage is obtained by setting I=0:

$$V_o = \frac{AkT}{e} \ln \frac{I_L - I_o}{I_o}. \tag{24}$$

For an ideal diode A=1; for actual solar cells a summation of terms of the form given in equation (23), each term having different values of A and I_o is often used to fit the experimental curves. For temperatures near room temperature the portion of the curve near V_o usually fits the ideal diode well[12]. Under such circumstances the difference in V_o, ΔV_o, between two illuminations W_1 and W_2 is*

$$\Delta V_o = \frac{AkT}{e} \ln \frac{W_2}{W_1}, \tag{25}$$

again, with A=1. However, equations (21) and (22) show ΔV_o to be independent of temperature. This corresponds to an A factor in equation (25) that is inversely proportional to cell temperature. An inverse temperature dependence of A has previously been suggested by Barrett et al[13] based on low temperature measurements by Kennerud[14]. In interpreting the present results as implying such a temperature dependence, a stipulation must be made, i.e., the measurements cover different illuminations in different temperature ranges. Thus it would be improper to use equation (21) or (22) for T/W combinations not measured, e.g., 423°K/35mW/cm^2 or 273°K/560mW/cm^2.

c. Quality of Experimental Fit

Since the experimental uncertainty of the measurements was essentially constant at ± 0.012V, the quality of the empirical fit was tested by calculating the difference, E, between data and equation directly in volts. The number of points for which this difference is greater than E_o, i.e., $N(|E| > |E_o|)$, is plotted versus E_o in Figures 31 and 32 for 10 Ω-cm cells and 1 Ω-cm cells, respectively. (These figures include all V_o data for T ≥ 223°K with the exception of 1 Ω-cm cell data at 5mW/cm^2, 223°K.)

Figure 31 indicates that for 10 Ω-cm cells the fits to all data points at 5, 35, and 560mW/cm^2 are within the experimental uncertainty of the measurements. At 140mW/cm^2 one reading differs from the equation by 0.017V, the equation giving the higher value. However, this data point was at 223°K, where Schottky barrier effects begin to reduce V_o. Similarly at 1830mW/cm^2 one reading

*It is assumed here that I_L is approximately proportional to W.

differs from the equation by 0.017V, the equation value being lower. This occurred for the cell block irradiated to 1×10^{15}e/cm^2. The reason for this large difference is not understood, however, the other two data points at this fluence and illumination were also higher than the values predicted by the equation (by 0.012V).

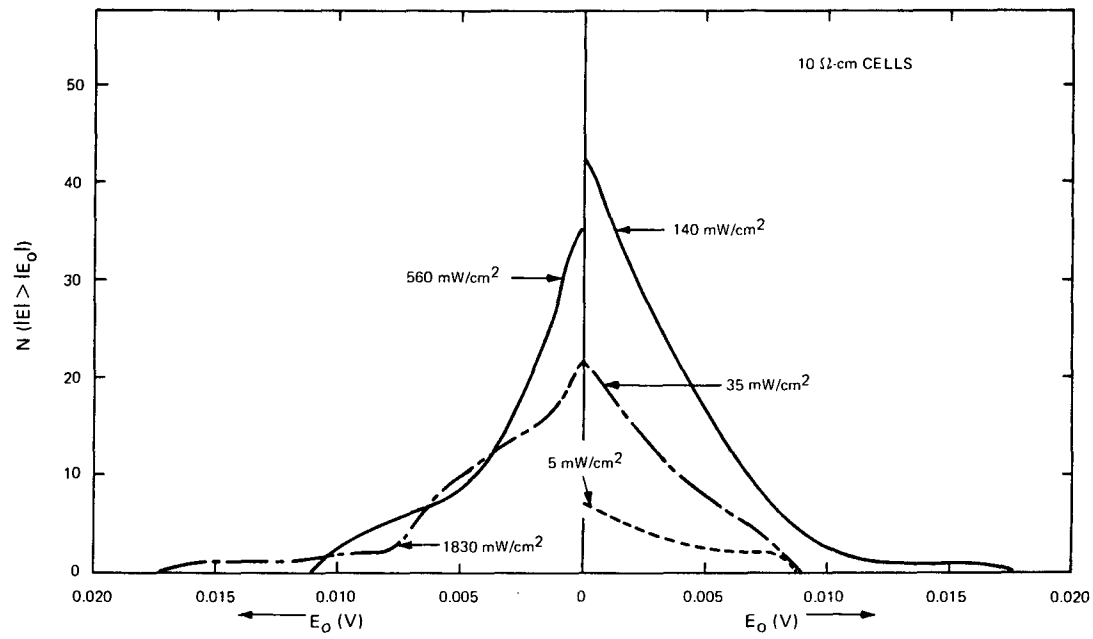

Figure 31. Divergence of V_o Values of Empirical Equations from Experimental V_o Values, 10 Ω-cm Cells

The fits for 1 Ω-cm cells are not as good, as is indicated in Figure 32. The number of readings for which the empirical voltage equation differs from the corresponding experimental point by more than 0.012V are:

3 of 42 points for 140mW/cm^2,

2 of 21 points for 35mW/cm^2,

8 of 34 points for 560mW/cm^2,

4 of 21 points for 1830mW/cm^2.

All three of these points for 140mW/cm^2 and both points for 35mW/cm^2 are on the cell group irradiated to 1×10^{14}e/cm^2 which is considered suspect due to its unusual high-temperature behavior. It is thus suggested that these five data points should be neglected, and the fit considered satisfactory at 140mW/cm^2 and 35mW/cm^2.

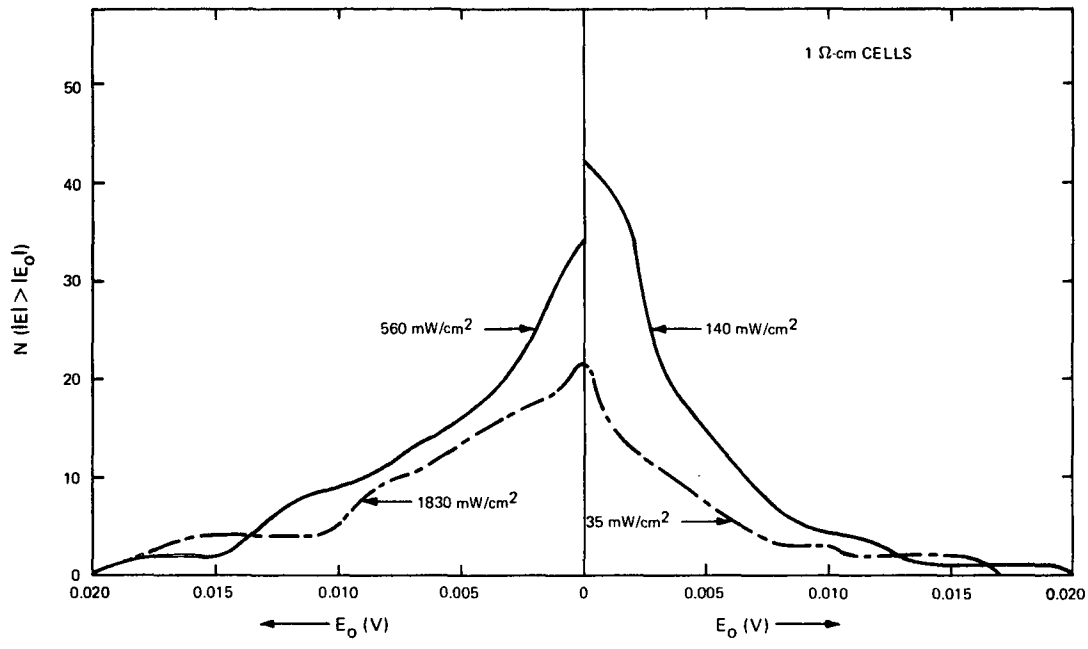

Figure 32. Divergence of V_o Values of Empirical Equations from Experimental V_o Values, 1 Ω-cm Cells

At 560mW/cm^2, only two of the points are at 1×10^{14}e/cm^2, leaving six points for which the fit is unsatisfactory. Two of these points appear in each of Figures 29 and 30, in each case they are at 273°K and 323°K. In Figure 29 ($\phi = 3 \times 10^{15}$e/cm^2) the equation gives higher values than the data while the reverse is true in Figure 30 ($\phi = 1 \times 10^{16}$e/cm^2). Examination of these figures shows that the data suggests an increase in the temperature coefficient, C_T, at 3×10^{15}e/cm^2 followed by a decrease in C_T at 1×10^{16}e/cm^2. It is considered unlikely that such a double reversal really occurs and it is therefore concluded that the empirical equation is adequate at 560mW/cm^2.

The points with poor fits at 1830mW/cm^2 do follow a pattern. The equation (slightly) overestimates V_o at 373°K and underestimates V_o at 473°K. Figures 29 and 30 illustrate this. Thus it is concluded that at this intensity the temperature coefficient for 1 Ω-cm cells is significantly lower than the equation indicates.

3. Voltage Anomaly at Low Temperature

The presence of a Schottky barrier at the back contact of the cell results in anomalous behavior at low temperatures. An example is shown in Figure 33 which gives the I-V curves for cell 12-4 before and after irradiation to a fluence of 3×10^{14}e/cm^2. The cell temperature is 173°K; the illumination, 140mW/cm^2. It is seen that the value of open-circuit voltage is greater after

irradiation than that before irradiation. This reversal of normal behavior was observed in most cells for the range: $T < 223°K$, $\phi \leq 1 \times 10^{15} e/cm^2$. The crossover in voltage occurs near open circuit voltage when the curve slope of the irradiated cell changes. It is suggested that this change in slope occurs because the voltage across the Schottky barrier is approaching zero. In contrast the unirradiated cell experiences little change in slope. It is thought that this is because a significant voltage appears across the barrier of the unirradiated cells, even at open-circuit voltage. This implies that the barrier itself is illuminated, i.e., there is a photovoltage across the barrier which subtracts from the cell photovoltage. In irradiated cells this photovoltage apparently approaches zero, and the Schottky barrier behaves more like an unilluminated diode.

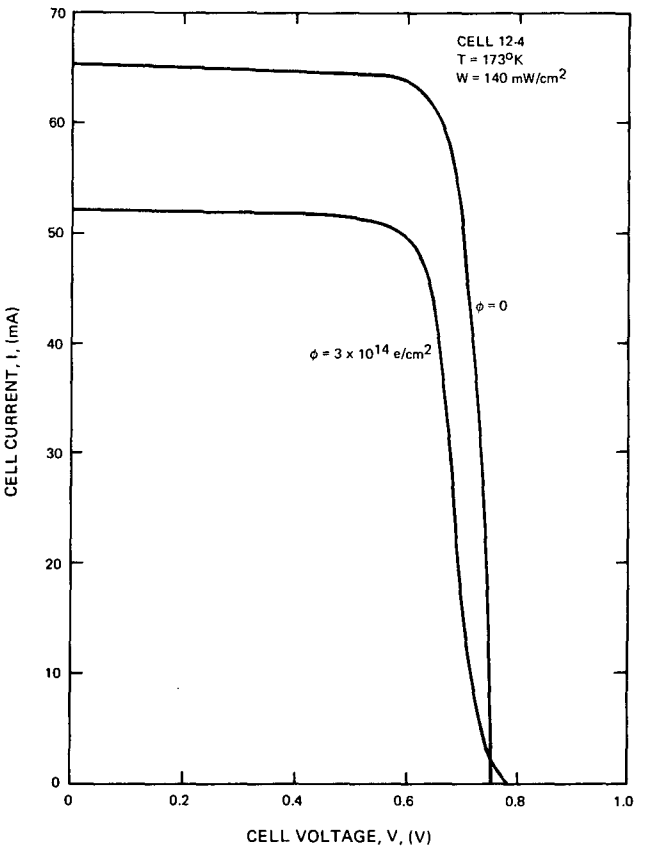

Figure 33. Photovoltaic Curves Showing the Effect of a Schottky Barrier at Low Cell Temperature

D. CURVE SHAPE

1. Range of Analysis

Cell design parameters vary in accordance with the projected range of application. The design of the cells used in these experiments fits the requirements of earth-orbit environments, where cell temperatures range from approximately

200°K to 370°K. The most applicable data was thus obtained in the temperature range from 223°K to 373°K. Accordingly, efforts in curve analysis were concentrated in this range, with cell illumination intensities of 35, 140, and 560mW/cm^2. Time constraints further limited the analysis to 10 Ω-cm cells.

2. Equation Format

Open circuit voltage provides a convenient starting point for analysis of the I-V curve. In equation (23), $I_F = I_L$ and IR_s=O at open-circuit voltage, consequently the coordinates (V_o, I_L) provide a point on the n/p junction characteristic which is not complicated by a series resistance term[12]. Since measurements were made at three illuminations three such points could be obtained from the data for each temperature and fluence. Plots of V_o versus I_L are given in Figure 34 for temperatures of 223, 273, 323, and 373°K, and fluences of 1×10^{13}, 3×10^{13}, 3×10^{14} and 1×10^{16}e/cm^2. The lines drawn through the data points each represent an open-circuit voltage difference, ΔV_o, for two different light-generated currents, I_{L1}, and I_{L2}, given by

$$\Delta V_o = 0.0265 \ln \frac{I_{L2}}{I_{L1}} . \qquad (26)$$

This is similar to the voltage difference given in terms of illumination, i.e., $\Delta V_o = 0.025 \ln (W_2/W_1)$, the slightly different coefficients being due to the apparent nonlinearity of I_L between 140 and 560mW/cm^2 illumination. As shown in Figure 34, all the data except those giving the low-temperature (223°K and 273°K) values for the lightest irradiation (1×10^{13}e/cm^2) fit equation (26) well. The implication is, as in the equation for V_o, that the empirical A factor is inversely proportional to temperature.

The voltage difference given in equation (26) forms the basis for the empirical current-voltage equation. A term is added to account for the cell series resistance, R_s, giving an equation of the form

$$V = V_o - 0.0265 \ln\left[\frac{I_L}{I_L - I}\right] - IR_s. \qquad (27)$$

where I_L and V_o are obtained from the equations developed in sections IIIB. and IIIC., respectively. Since the validity of equation (26) is limited to the range of the V_o measurements it doesn't necessarily provide a true zero resistance base line at voltages smaller than the lowest V_o measurement. Consequently R_s is not the true series resistance of the cell. However this will not effect the empirical validity of equation (27). Empirical relationships for R_s are developed below.

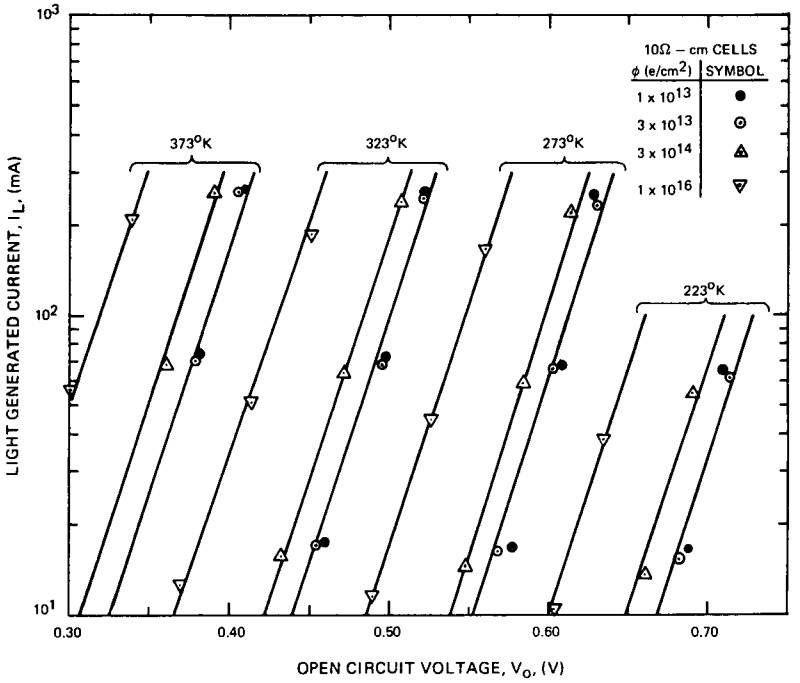

Figure 34. Open Circuit Voltage Versus Light Generated Current at Several Fluences and Cell Temperatures, 10 Ω-cm Cells

3. Series Resistance

The parameter R_S is a function of all the variables of the experiment, i.e., T, W, and ϕ, and in addition varies along the I-V curve. The method used to calculate R_S as a function of cell voltage is illustrated in Figure 35 in which the current, I_L-I, is plotted versus cell voltage for cell 13-3 at 273°K and 560mW/cm^2 illumination. The I-V curve (the curve on the left) was re-plotted on this semilog scale from the experimental I-V curve, the straight line through the (V_O, I_L) coordinates represents the base line provided by equation (26). The value of R_S at any voltage, V, is the voltage difference, ΔV, between the curve and the base line, divided by the current, I. By repeating this procedure for a series of cell voltages an R_S versus voltage characteristic is generated.

This technique was applied to individual cells at each of five fluences: 3×10^{13}, 3×10^{14}, 1×10^{15}, 3×10^{15}, and 1×10^{16}e/cm^2 and three temperatures, 273°, 323° and 373°K.* The results for 273°K and 373°K are shown in Figures 36 and 37, respectively, in which R_S is plotted versus V_O-V for each of the five fluences. R_S is seen to increase approximately linearly with V_O-V, the slope being independent of fluence, and the intercept with the R_S axis increasing with fluence. (The dependence on V is in general agreement with results previously reported for unirradiated cells[15].)

*In computing the R_S versus voltage characteristic, the I-V curves for 560mW/cm^2 illumination were used because they have larger values of ΔV than the lower illuminations and consequently greater accuracy.

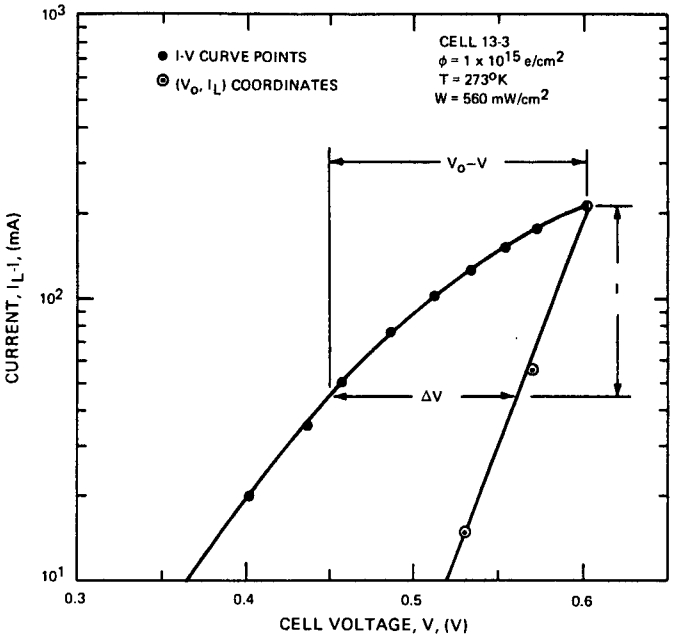

Figure 35. Illustration of Method for Calculating R_S

Fluence dependence of R_S is shown in Figure 38 for the three temperatures for which it was computed. The value of V_O-V=0.175V was chosen since it represented a point on the curve close to the maximum power point. The fluence dependence is reasonably close to logarithmic; there is also an increase in R_S with increasing temperature. Similar plots are shown in Figures 39 and 40 for illuminations of 140mW/cm^2 and 35mW/cm^2, respectively. In these figures each experimental point represents the average of values for two different cells. The calculations were made for V_O-V values of 0.100V and 0.080V for illuminations of 140mW/cm^2 and 35mW/cm^2, respectively, because those values were close to the maximum power point. There is a great deal of scatter in the computed values, especially for 35mW/cm^2 where ΔV was small and the experimental uncertainty correspondingly large. However, the dependencies are generally similar to those shown in Figure 38. Two additional features are apparent, a minimum in R_S at T=273°K, and an increase with decreasing illumination.

All of this data was combined to yield an empirical equation giving dependencies on T, W, ϕ, and V_O-V:

$$R_S = \left(\frac{110}{W-30}\right)^{0.23} \left[0.133 \log_{10} \phi + 1.87\,(V_O-V) + 2 \times 10^{-5}\,(T-273)^2 - 1.32\right]. \quad (28)$$

The $(V-V_O)$ dependence was obtained from the results illustrated in Figures 36 and 37, i.e., from computations at 560mW/cm^2. The remaining dependencies were based on the data at all three illuminations. Equation (28) is plotted in Figures 38-40 for each of the temperatures covered. The high degree of scatter in the data, especially in Figure 40, renders their description by an equation rather presumptuous. Still, the equation provides a reasonable fit to the data, such as it is. For 560mW/cm^2 the largest difference

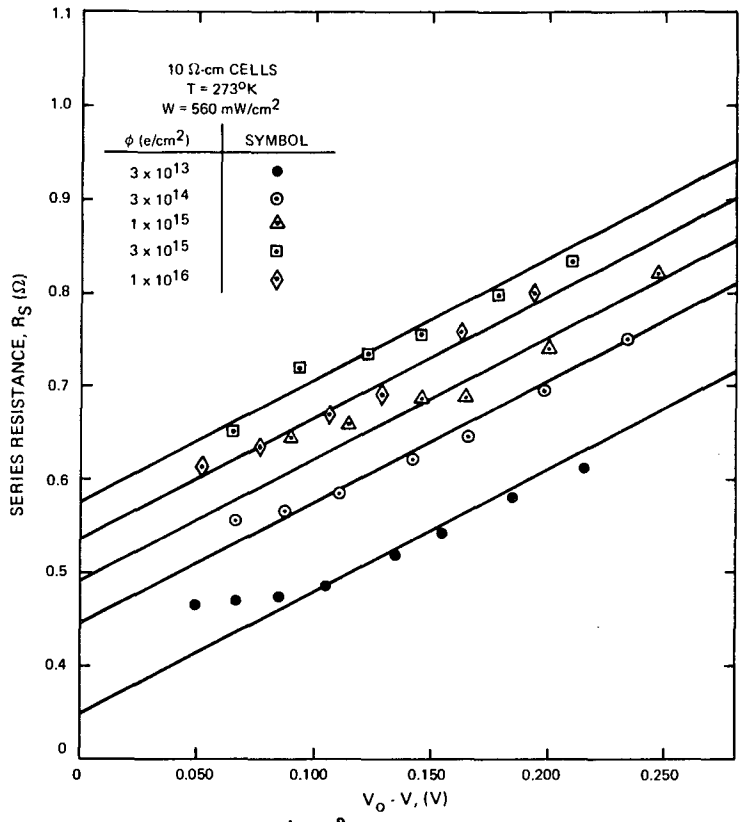

Figure 36. R_S at 560 mW/cm^2 Versus Position on the Solar-Cell Photovoltaic Characteristic, T = 273°K

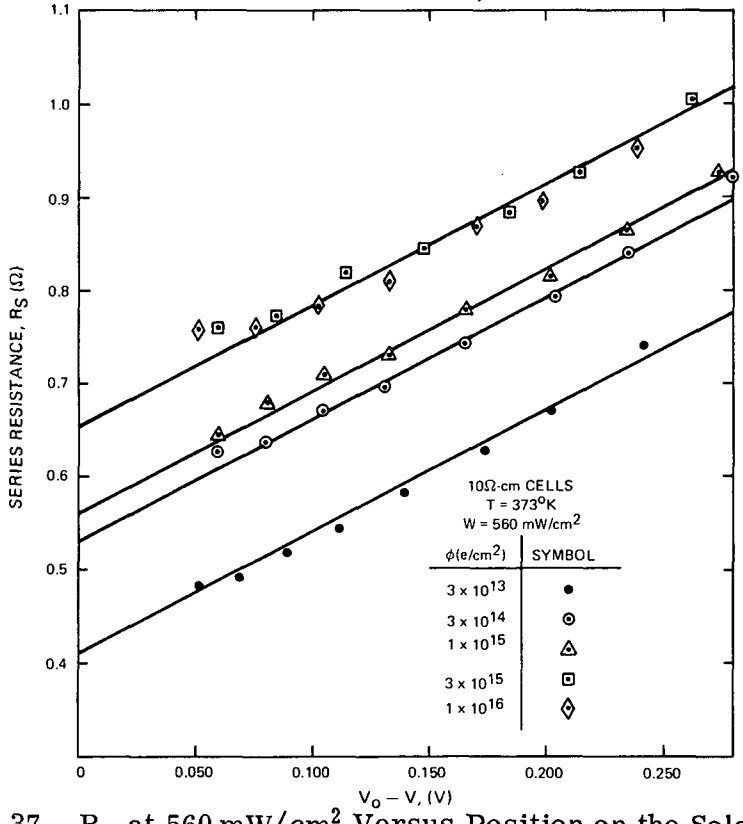

Figure 37. R_S at 560 mW/cm^2 Versus Position on the Solar-Cell Photovoltaic Characteristic, T = 373° K

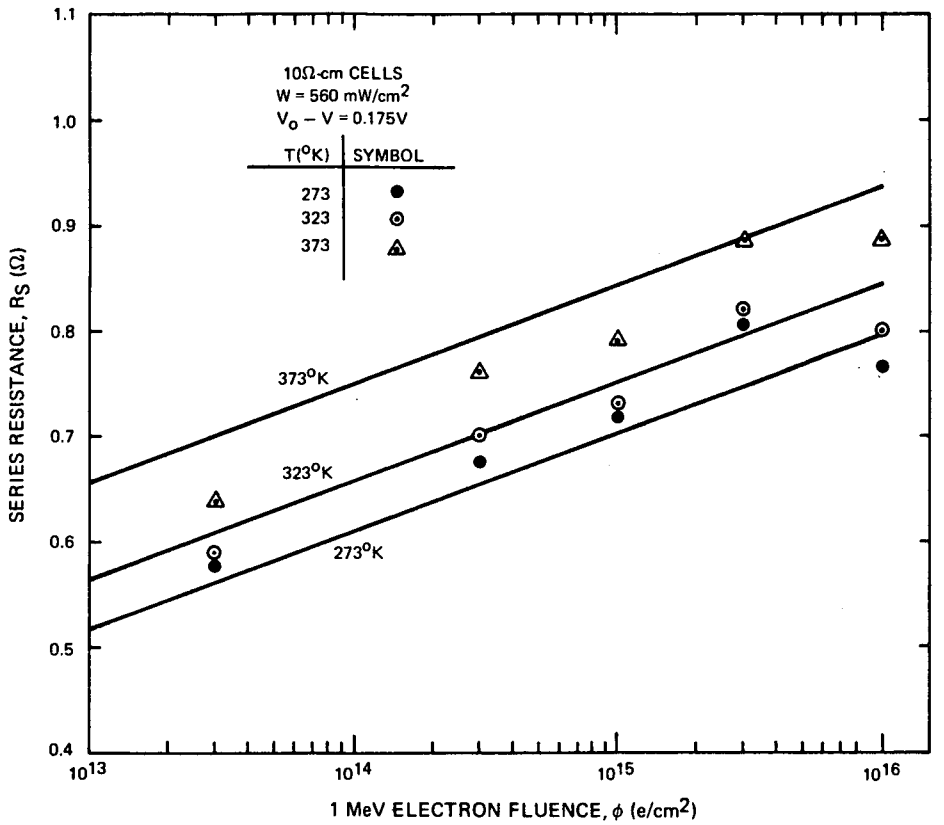

Figure 38. R_S Versus Fluence and Cell Temperature, W=560mW/cm^2

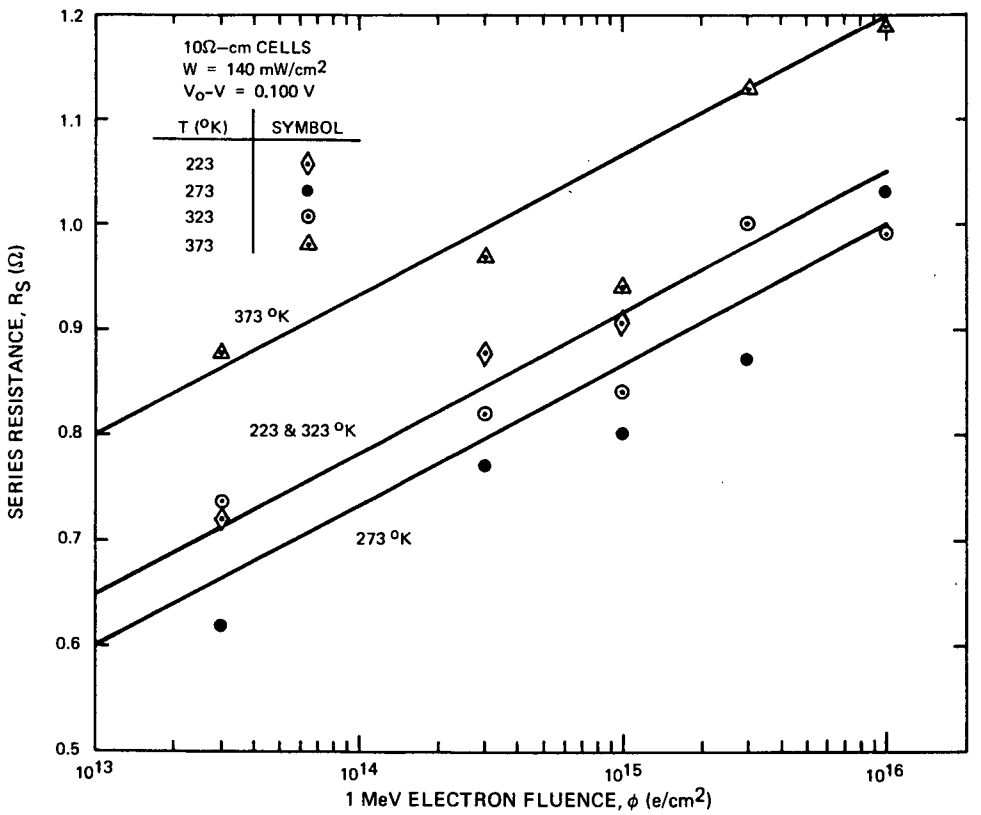

Figure 39. R_S Versus Fluence and Cell Temperature, W=140mW/cm^2

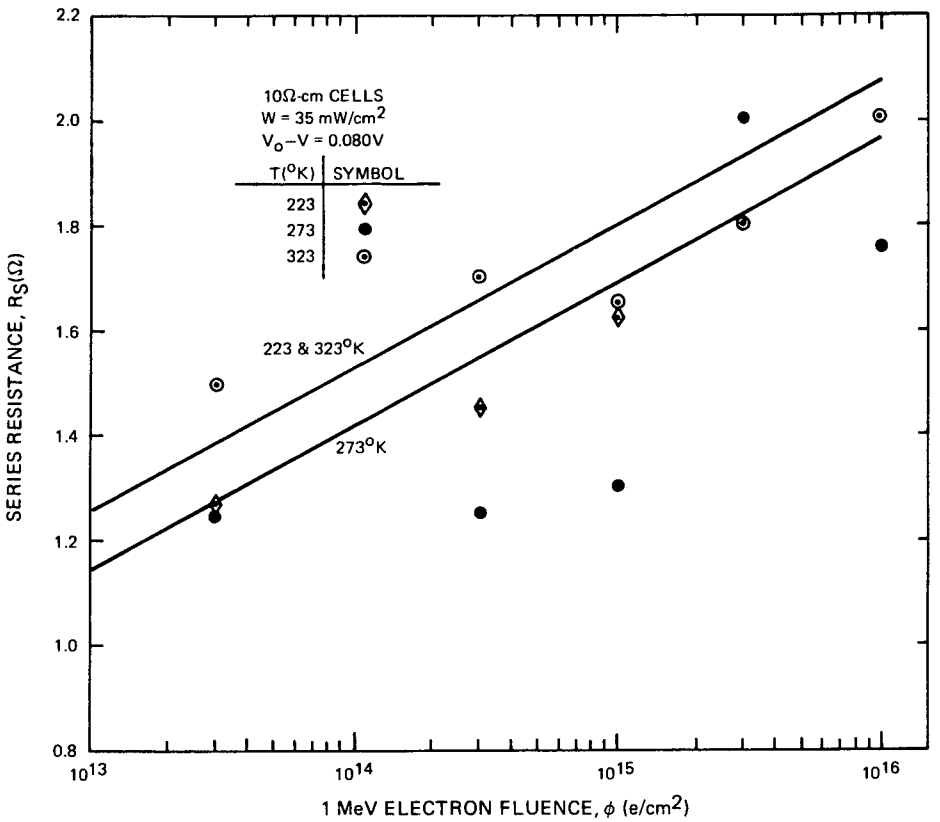

Figure 40. R_S Versus Fluence and Cell Temperature, W=35mW/cm^2

between the equation and a corresponding data point is 0.06 Ω. The corresponding numbers for 140mW/cm^2 and 35mW/cm^2 are 0.12Ω and o.36Ω. Cell to cell variations at the respective illuminations are higher than these differences.

Figure 41 illustrates the results obtained by applying the R_S versus voltage dependence of equation (28). The experimental I-V curve points are shown for cell 12-4 at 273°K, together with curves generated using equation (28), and curves generated using a constant resistance value established by matching to the experimental data at the maximum power point. The curves obtained from equation (28) provide a good fit except at low values of I_L-I, i.e., except below the knee of the curve near the short-circuit current point. In this low-voltage region of the curve high A-factors are customarily fitted by the addition of an exponential term in the diode equation, equation (23). In the present experiments this portion of the I-V curve was noisy due to a fluctuation in the xenon arc of the illuminator (section IIB). Consequently the quality of the data at low voltages did not warrant further refinement of the empirical equations.

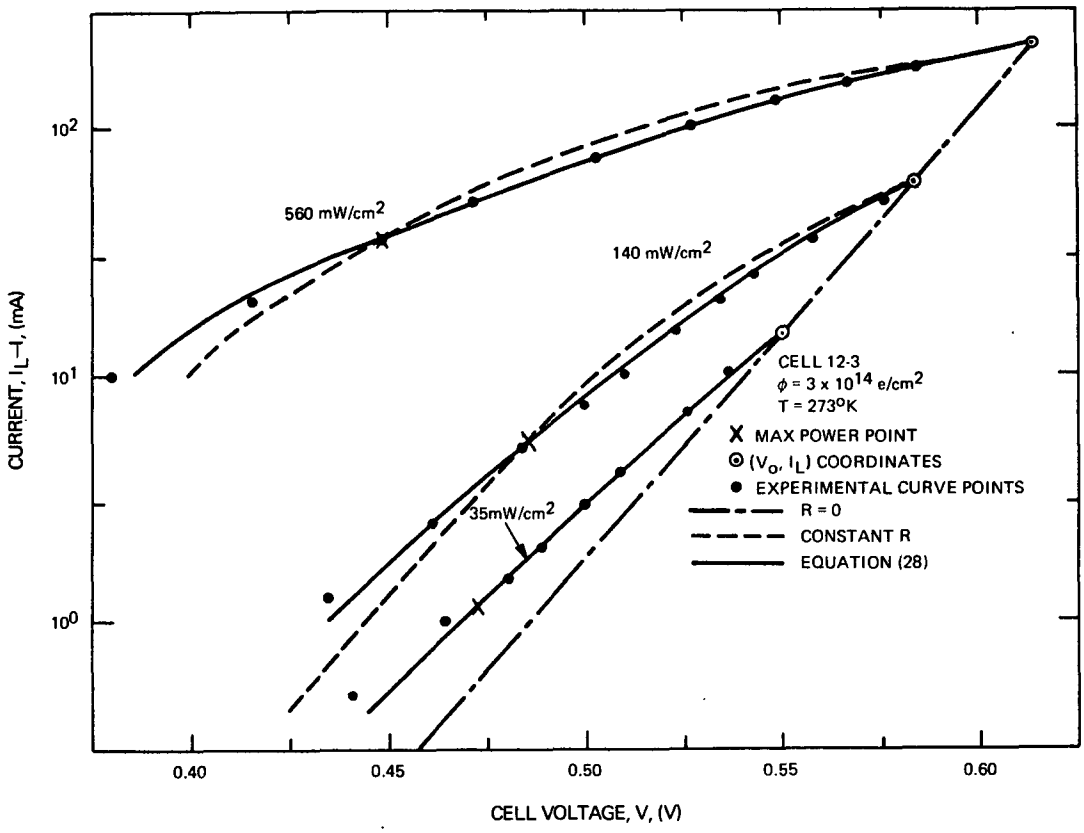

Figure 41. Illustration of Fit Between Empirical and Experimental I-V Curves

The current-voltage relationship for 10 Ω-cm cells is obtained by combining equations (27) and (28). The result is:

$$V = \frac{1}{1-1.87\ I\left(\frac{110}{W-30}\right)^{0.23}} X$$

$$\left\{ V_o - 0.0265 \ln\left(\frac{I_L}{I_L - I}\right) + \left(\frac{110}{W-30}\right)^{0.23} I \left[0.133 \log_{10} \phi + 1.87\ V_o + 2 \times 10^{-5} (T-273)^2 - 1.32 \right] \right\}, \qquad (29)$$

where V_o is obtained from equation (21) and I_L from equations (10), (14), and (15) for illuminations of 140mW/cm², 35mW/cm², and 560mW/cm², respectively. Cell output power, P, (in mW) at any voltage, V, is obtained by multiplying equation (29) by the current, I. The maximum power point is readily obtained by setting the derivative dP/dV=O, which results in a transcendental equation in I.

4. Curve-Shape Temperature Dependence

It is implicit in equation (27) that the I-V curve shape is invariant, except for the IR_S term, with respect to temperature, i.e., that curves of the same cell at different temperatures will align after translations of the I and V axis if $R_S = 0$, or, if $(IR_S)_{T_1} = (IR_S)_{T_2}$. The second of these conditions is approximately met for $T_1 = 223°K$ and $T_2 = 323°K$ since the R_S values were found to be similar (see equation (28)) at these two temperatures. To test equation (27) several tracings of I-V curves were made at these two temperatures. Three of these are shown in Figures 42-44. The similarity in curve shapes is evident, translation of axes showing the knee of each curve at 223°K to align well with that of the corresponding 323°K curve. For the sake of comparison Figure 45 shows (series-resistance free) curves constructed for 223°K and 323°K with a temperature-independent A factor of 1.36 (the approximate value of A for the real curves at T=223°K). The difference in curve shapes at the two temperatures is evident. This implies that the inverse relationship between cell temperature and the empirical A factor provides a fair approximation in this temperature range.

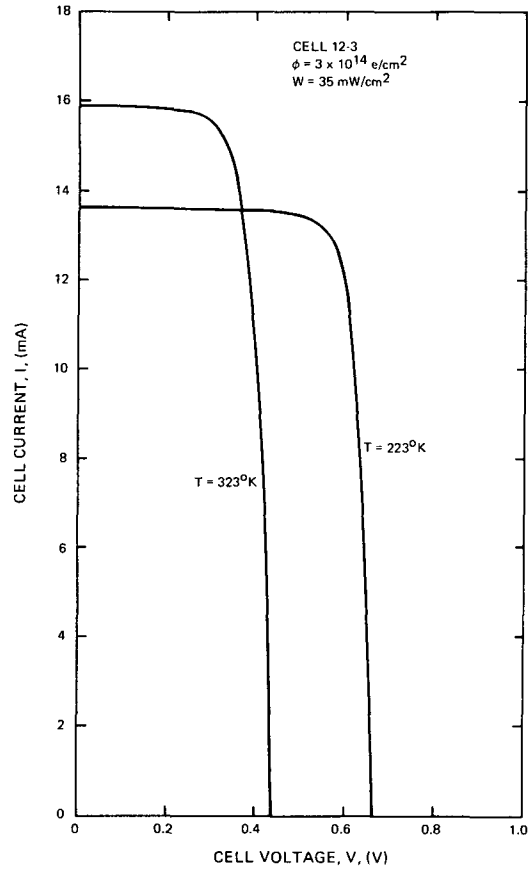

Figure 42. Photovoltaic Characteristics at W = 35mW/cm^2, $\phi = 3 \times 10^{14}$e/cm^2

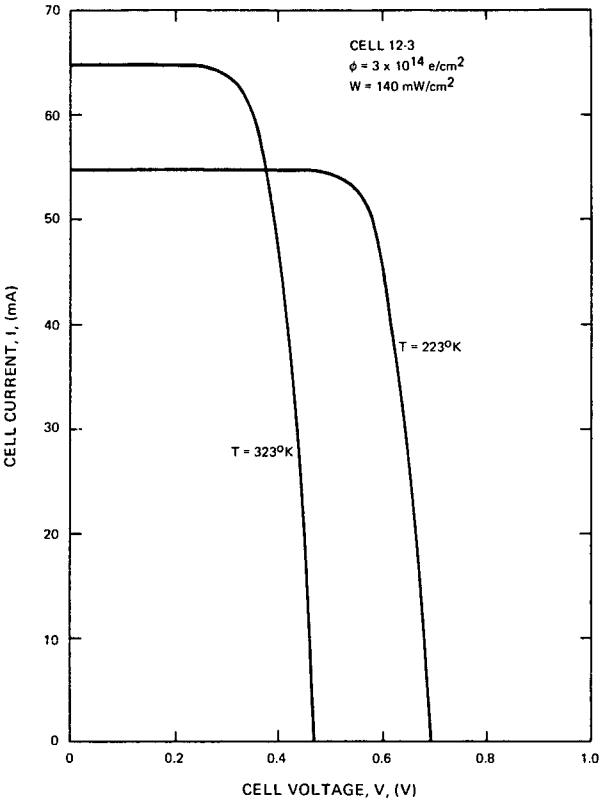

Figure 43. Photovoltaic Characteristics at W = 140mW/cm^2, ϕ = 3 x 10^{14}e/cm^2

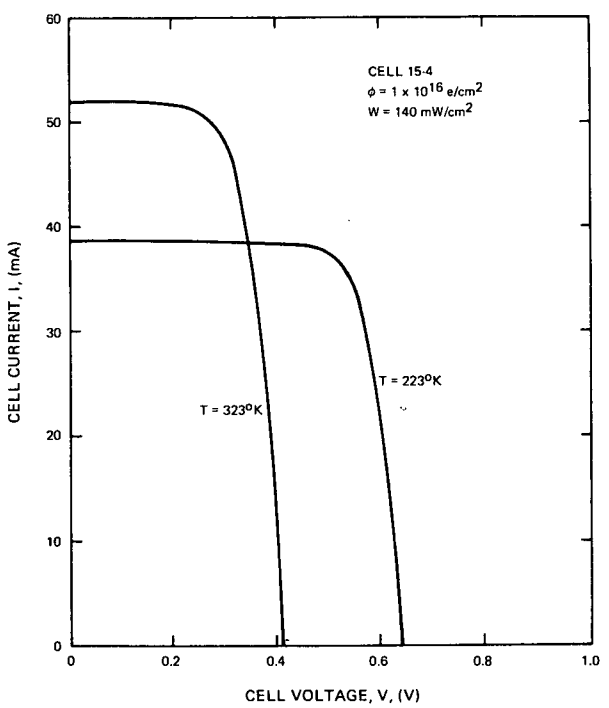

Figure 44. Photovoltaic Characteristics at W = 140mW/cm^2, ϕ = 1 x 10^{16}e/cm^2

E

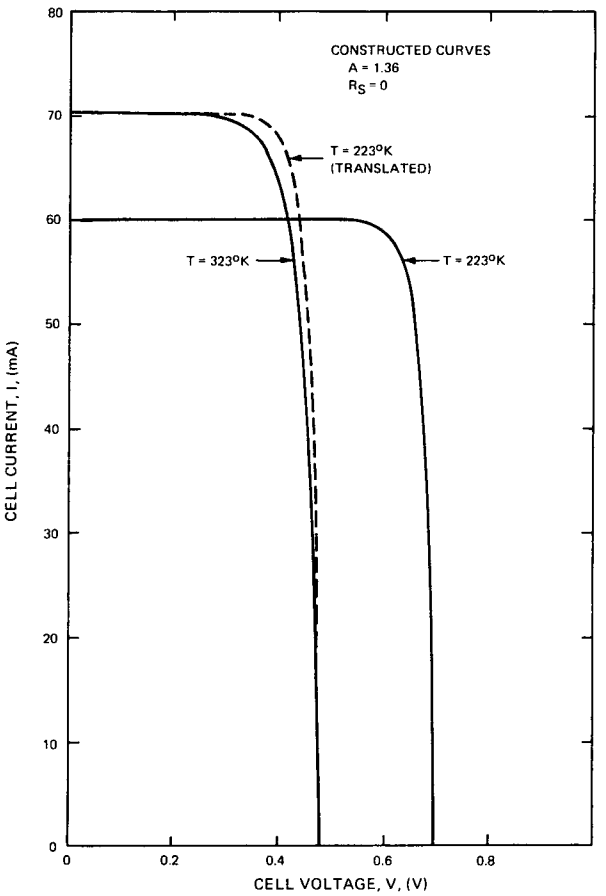

Figure 45. Constructed Photovoltaic Characteristics (using A = 1.36)

IV. CONCLUSIONS

Photovoltaic characteristics have been measured on solar cells irradiated by 1 MeV electrons to fluences ranging from 1×10^{13}e/cm^2 to 1×10^{16}e/cm^2, for cell temperatures ranging from 123°K to 473°K and illumination intensities ranging from 5mW/cm^2 to 1830mW/cm^2. Empirical equations have been derived from these measurements to describe the behavior of light generated current, open circuit voltage and I-V curve shape over various portions of these temperature/illumination (T/W) ranges. Both 10Ω-cm and 1Ω-cm n/p silicon solar cells were tested, similar analytical expressions being sought to provide a basis for easy comparisons between the two resistivities.

Equations for light generated current were obtained for both resistivities covering the entire experimental T/W range. The temperature dependencies are similar for both resistivities at high temperature ($T \geq 273°K$) the normalized temperature coefficient varies with fluence as $\phi^{0.18}$, at low temperature the coefficient is relatively independent of fluence. Two different forms were derived for fluence dependence at T = 273°K, the customary logarithmic form and a power law relationship. Both forms fitted the data well but the logarithmic form required at least one change of coefficients to cover the fluence range while a single power law expression, with current decreasing as $\phi^{0.153}$ for both resistivities, fitted the entire range. The coefficient of the power law expression was larger for 1Ω-cm cells, consequently the advantage in current for 10Ω-cm cells increased with increasing fluence.

Open circuit voltage equations have been derived for all temperatures except 123°K and 173°K, where Schottky barrier effects and cell (high A factor) shunting led to questionable experimental results. The temperature coefficient of voltage was, to a reasonable approximation, independent of temperature and illumination for both resistivities and for 10Ω-cm cells was 0.0023 V/°K independent of fluence. For 1 Ω-cm cells it was 0.0022 V/°K for low fluences and 0.0023 V/°K for fluences of 3×10^{14}e/cm^2 and above. Illumination dependence was logarithmic, the voltage increasing by approximately 0.025 V and 0.032 V per decade increase in illumination for 10 Ω-cm cells and 1Ω-cm cells, respectively. At T = 273°K, the decrease with fluence varied as $\phi^{0.25}$ for both resistivities. At 140mW/cm^2 the voltage difference between 1 - and 10Ω-cm cells, as given by the equations, is constant at 0.030 V (independent of temperature) for $\phi \geq 3 \times 10^{14}$e/cm^2. Since the illumination dependence is stronger in the 1Ω-cm cells, this 0.030 V advantage increases at high intensity and decreases at low intensity.

An equation for the entire I-V curve was generated for 10Ω-cm cells for temperatures between 223°K and 373°K and illuminations of 35, 140, and 560mW/cm^2. This covered the entire T/W span for which the cells used in the experiments were designed. (For low temperature applications cells incorporate p^+ regions adjacent to the back contact to avoid Schottky - barrier diode formation; for high temperature applications cells have low base resistivity, deep junction

diffusions, and extra contact fingers to minimize series resistance.) The equation was based on the illumination-dependent open-circuit voltage equation with a term added to account for a resistance drop across the cell. The experimental curves were fit well using a (ficticious) series resistance which depended on temperature, illumination, fluence, and voltage offset from open circuit voltage. The empirical I-V equation and the open circuit voltage equation both imply an inverse temperature dependence of the empirical A factor customarily used in solar cell I-V equations. Such dependence results in a curve shape near maximum power which is invariant with temperature. This was found to be a good approximation in checks of the experimental data.

Resistivity comparisons indicate low base resistivity, 1 Ω-cm, cells to be superior for high temperature, high illumination applications. High resistivity, 10 Ω-cm, cells are superior for low temperature, low illumination applications. For intermediate T/W values, a detailed knowledge of mission parameters and requirements is needed to determine the better resistivity.

V. ACKNOWLEDGEMENTS

The writer wishes to acknowledge the encouragement and support of A. F. Obenschain and D. Harris of NASA-GSFC and of P. Nekrasov of RCA, and the helpful discussions of G. Brucker. T. Glock, R. Neadle, and W. Rutan provided capable support in the design and fabrication of experimental apparatus and in the performance of measurements. P. Pierce, now at EOS, collaborated in the early stages of the program. Cell irradiations were performed by J. Groppe of RCA Laboratories.

VI. REFERENCES

1. F.S. Johnson , Journal of Meteorology 2, 6 (1954).
2. D.W. Ritchie, Proc. Fourth Photovoltaic Spec. Conf. Volume II, PIC-SOL 209/5.1, August 1964.
3. C.A. Lewis and J.P. Kirkpatrick, Conf. Record of Eighth Photovoltaic Spec. Conf., IEEE catalog No. 70C 32 ED, 123 (1970).
4. P.A. Iles, Final Report, JPL Contract No. 952865, issued by Centralab Div. of Globe - Union Inc., Nov. 30, 1971.
5. C.T. Sah, R.N. Noyce, and W. Shockley Proc. IRE 45, 1228 (1957).
6. H.W. Brandhorst and R.E. Hart, Conf. Record of Eighth Photovoltaic Spec. Conf., IEEE catalog No. 70C 32 ED, 142 (1970).
7. J.C. Ho, F.T.C. Bartels, and A.R. Kirkpatrick, Conf. Record of Eighth Photovoltaic Spec. Conf., IEEE catalog No. 70C 32 ED, 150 (1970).
8. W. Luft, Conf. Record of Eighth Photovoltaic Spec. Conf. IEEE catalog No. 70C 32 ED, 161 (1970).
9. P.A. Payne and E.L. Ralph, Conf. Record of Eighth Photovoltaic Spec. Conf., IEEE catalog No. 70C 32 ED, 135 (1970).
10. P.H. Fang, NASA Goddard Space Flight Center, X-713-65-468, November 1965.
11. E.L. Ralph, Conf. Record of Sixth Photovoltaic Spec. Conf., IEEE catalog No. 15C53 Volume I, 98 (1967).
12. M. Wolf and H. Rauschenbach, Adv. Energy Conversion, 3, 455 (1963).
13. M.J. Barrett, M.B. Hornstein and R.H. Stroud, Final Report, JPL Contract No. 952548, prepared by Exotech Inc. June 15, 1970.
14. K.L. Kennerud, IEEE Trans. on Aerospace and Electronic Systems, AES-3, 586 (July 1967).
15. M.S. Imamura and J.I. Portscheller, Conf. Record of Eighth Photovoltaic Spec. Conf., IEEE catalog No. 70C 32 ED, 102 (1970).

VII. APPENDIX

A. GLOSSARY

The symbols used in the text and their definitions are listed below:

A	empirical fitting factor in diode equation
C_T	open-circuit-voltage temperature coefficient (V/°K)
e	electron charge (1.6×10^{-19}C)
I	solar-cell current (mA)
I_F	diode forward current (mA)
I_L	light generated current (mA)
I_L (T, W, ϕ)	light generated current - see Table A-1
I_o	diode reverse saturation current (mA)
I_{sc}	short circuit current (mA)
k	Boltzmann's constant (1.38×10^{-23} J/°K)
P	solar-cell power (mW)
R_S	series resistance (Ω)
T	solar-cell temperature (°K)
V	solar-cell voltage (V)
V_o	open circuit voltage (V)
V_o (T, W, ϕ)	open circuit voltage - see Table A-1
W	intensity of illumination (mW/cm^2)
ϕ	1 MeV electron fluence (e/cm^2)
ξ_W	ratio of I_L at intensity W to I_L at intensity of 140mW/cm^2

E, I_D, I_E, γ, δ_I, δ_V, χ, λ_ϕ - defined as used in text

The symbols I_L and V_O are often followed by parentheses to indicate specific dependence on (T, W, ϕ). To identify a specific value for one of these variables, an index number is used instead of the symbol. The index numbers and the values of T, W, and ϕ they represent are listed in Table A-I. Index numbers run from 1 to 8 for T, from 1 to 5 for W, and from 1 to 7 for ϕ. A combination used frequently in the text is I_L $(4, 3, \phi)$ which is the light generated current at T=273°K, and W=140mW/cm^2, as a function of fluence, ϕ.

TABLE A-I. INDEX NUMBERS AND CORRESPONDING VALUES FOR THE PARAMETERS T, W, AND ϕ

Index No.	1	2	3	4	5	6	7	8
Temperature, T, (°K)	123	173	223	273	323	373	423	473
Illumination, W, (mW/cm^2)	5	35	140	560	1830	-	-	-
Fluence, ϕ, (e/cm^2)	1×10^{13}	3×10^{13}	1×10^{14}	3×10^{14}	1×10^{15}	3×10^{15}	1×10^{16}	-